Physics of the Earth and Planetary Interiors 268 (2017) 18–34

Contents lists available at ScienceDirect

Physics of the Earth and Planetary Interiors

journal homepage: www.elsevier.com/locate/pepi

Hot climate inhibits volcanism on Venus: Constraints from rock deformation experiments and argon isotope geochemistry

Sami Mikhail [a,b,*], Michael J. Heap [c]

[a] The School of Earth and Environmental Sciences, The University of St. Andrews, St. Andrews, UK
[b] St. Andrews Centre for Exoplanet Science, The University of St. Andrews, UK
[c] Géophysique Expérimentale, Institut de Physique de Globe de Strasbourg (UMR 7516 CNRS, Université de Strasbourg/EOST), 5 rue René Descartes, 67084 Strasbourg Cedex, France

ARTICLE INFO

Article history:
Received 20 July 2016
Received in revised form 19 December 2016
Accepted 3 May 2017
Available online 6 May 2017

ABSTRACT

The disparate evolution of sibling planets Earth and Venus has left them markedly different. Venus' hot (460 °C) surface is dry and has a hypsometry with a very low standard deviation, whereas Earth's average temperature is 4 °C and the surface is wet and has a pronounced bimodal hypsometry. Counterintuitively, despite the hot Venusian climate, the rate of intraplate volcano formation is an order of magnitude lower than that of Earth. Here we compile and analyse rock deformation and atmospheric argon isotope data to offer an explanation for the relative contrast in volcanic flux between Earth and Venus. By collating high-temperature, high-pressure rock deformation data for basalt, we provide a failure mechanism map to assess the depth of the brittle–ductile transition (BDT). These data suggest that the Venusian BDT likely exists between 2 and 12 km depth (for a range of thermal gradients), in stark contrast to the BDT for Earth, which we find to be at a depth of ~25–27 km using the same method. The implications for planetary evolution are twofold. First, downflexing and sagging will result in the sinking of high-relief structures, due to the low flexural rigidity of the predominantly ductile Venusian crust, offering an explanation for the curious coronae features on the Venusian surface. Second, magma delivery to the surface—the most efficient mechanism for which is flow along fractures (dykes; i.e., brittle deformation)—will be inhibited on Venus. Instead, we infer that magmas must stall and pond in the ductile Venusian crust. If true, a greater proportion of magmatism on Venus should result in intrusion rather than extrusion, relative to Earth. This predicted lower volcanic flux on Venus, relative to Earth, is supported by atmospheric argon isotope data: we argue here that the anomalously unradiogenic present-day atmospheric $^{40}Ar/^{36}Ar$ ratio for Venus (compared with Earth) must reflect major differences in ^{40}Ar degassing, primarily driven by volcanism. Indeed, these argon data suggest that the volcanic flux on Venus has been three times lower than that on Earth over its 4.56 billion year history. We conclude that Venus' hot climate inhibits volcanism.

1. Introduction

The present-day differences in the expression and intensity of volcanism on the telluric planets serves as a testament to the dynamic nature of planetary evolution (Wilson, 2009). For example, Earth and Venus are colloquially referred to as sibling planets because of their similar mass and bulk composition (i.e., bulk petrology). However, their contrasting atmospheric mass and chemistry (e.g., Gaillard and Scaillet, 2014; Mikhail and Sverjensky, 2014), climate (e.g., Pollack et al., 1980), geomorphology (e.g., Head and Solomon, 1981; Donahue and Russell, 1997; Basilevsky and Head, 2003; Ghail, 2015), and volcanic character (e.g., Fegley and Prinn, 1989; Head et al., 1992; Wilson, 2009) is striking: Earth is a crucible of life, whereas Venus is a barren wasteland. Suffice to say, then, Earth and Venus are not identical siblings. The major differences between Venus and Earth are discussed in detail below.

First, the average surface temperatures are 460 and 4 °C on Venus and Earth, respectively. The Earth also has an excess in surface water of about 1.2×10^{21} kg compared to Venus, a difference between five and six orders of magnitude (Donahue, 1999; Lécuyer et al., 2010). The high temperature and low water content of the Venusian surface are a combined consequence of the absence of a magnetic field (Donahue and Russell, 1997), the presence of a dense atmosphere dominated by CO_2 (at a pressure of 9 MPa), and its proximity to the Sun (with a solar irradiance of 2611 W/m^2, compared with 1366 W/m^2 on Earth).

* Corresponding author.
E-mail address: sm342@st-andrews.ac.uk (S. Mikhail).

http://dx.doi.org/10.1016/j.pepi.2017.05.007
0031-9201/

Second, hypsometric data show that >80% of the surface elevation of Venus ranges from −1.0 to +2.5 km; only ~2% of the surface lies >2 km above the median radius (Fig. 1) (Head and Solomon, 1981; Basilevsky and Head, 2003; Taylor and McLennan, 2009). The surface of Earth, by contrast, has a pronounced bimodal hypsometry (i.e., it has continental rises and ocean basins; Fig. 1). The fact that Venus has a hypsometry with a very low standard deviation is not easily attributable to the absence of plate tectonics on Venus, because Mars—a planet that, like Venus, operates a stagnant-lid tectonic regime (Head and Solomon, 1981; Head et al., 1992; Donahue and Russell, 1997; Basilevsky and Head, 2003)—has a surface hypsometry with a very large standard deviation (Fig. 1).

Third, the way in which volcanism is manifest on Earth and Venus differs substantially (e.g., Wilson and Head, 1983; Wilson, 2009). For example, while the majority (*ca.* 90%) of Earth's volcanism occurs along curvilinear belts and rift-margins, which collectively define tectonic plate boundaries (Cottrell, 2015), Venus operates a stagnant-lid tectonic regime and is dominated by features interpreted to be related to mantle plumes (e.g., Head et al., 1992). Although Venus hosts volcanic features commonly observed on Earth, such as lava plains, discrete lava flows, shield volcanoes, and shield fields, it is also home to enigmatic, flat landforms such as coronae (Head et al., 1992; Stofan et al., 1992; Squyres et al., 1992; McKenzie et al., 1992; Grosfils and Head, 1994; Addington, 2001; Krassilnikov and Head, 2003; Grindrod and Hoogenboom, 2006; Robin et al., 2007; Wilson, 2009; Krassilnikov et al., 2012; Ivanov and Head, 2013).

An important difference between volcanism on Earth and Venus is that, by comparing intraplate volcanic fluxes on both Earth and Venus, it is clear that Earth is the most volcanically active of the two planets, possibly by at least an order of magnitude (Ivanov and Head, 2013). Indeed, while intraplate volcanic activity on Earth is evidently abundant, evidence for ongoing, present-day volcanism on Venus is comparatively sparse, although it is thought that the vast majority of the Venusian surface is volcanic in origin (Head et al., 1992; Basilevsky and Head, 2003; Wilson, 2009). However, a number of recent findings suggest that volcanic activity on Venus persists to the present: [1] infrared radiation from three volcanic regions showed some flows to be warmer than their surrounding rocks, implying that these lavas are younger than 2.5 Ma (Smrekar et al., 2010); [2] sporadic atmospheric SO_2 fluctuations have been observed at Venus (Esposito, 1984; Marcq et al., 2011); and [3] thermal spikes have been reported at Ganiki Chasma, a rift valley proximal to Ozza and Maat Montes (Shalygin et al., 2015). In addition, the sulfuric clouds that envelop the entire planet would not persist beyond 1–50 Ma without the replenishment of SO_2, the source of which is presumed to be magmatic (Fegley and Prinn, 1989; Bullock and Grinspoon, 2001).

To emphasise the difference between volcanic activity on Earth and Venus: while Earth's oceanic crust (that covers 60% of Earth's surface) has created >100,000 individual volcanoes (including seamounts) in <100 Ma (e.g., Wessel, 2001 and references therein), Venus' entire surface has produced roughly 70,000 individual volcanoes in <700 Ma (Head et al., 1992). The difference in the rate of volcano production is therefore at least an order of magnitude greater on Earth than on Venus. We further note that, because >70% of all extrusive volcanism on Earth occurs beneath ocean depths >1000 m under pressures >9 MPa, the presence of coronae, a landform unique to the surface of Venus, cannot simply be explained by the high Venusian atmospheric pressure (Smith,

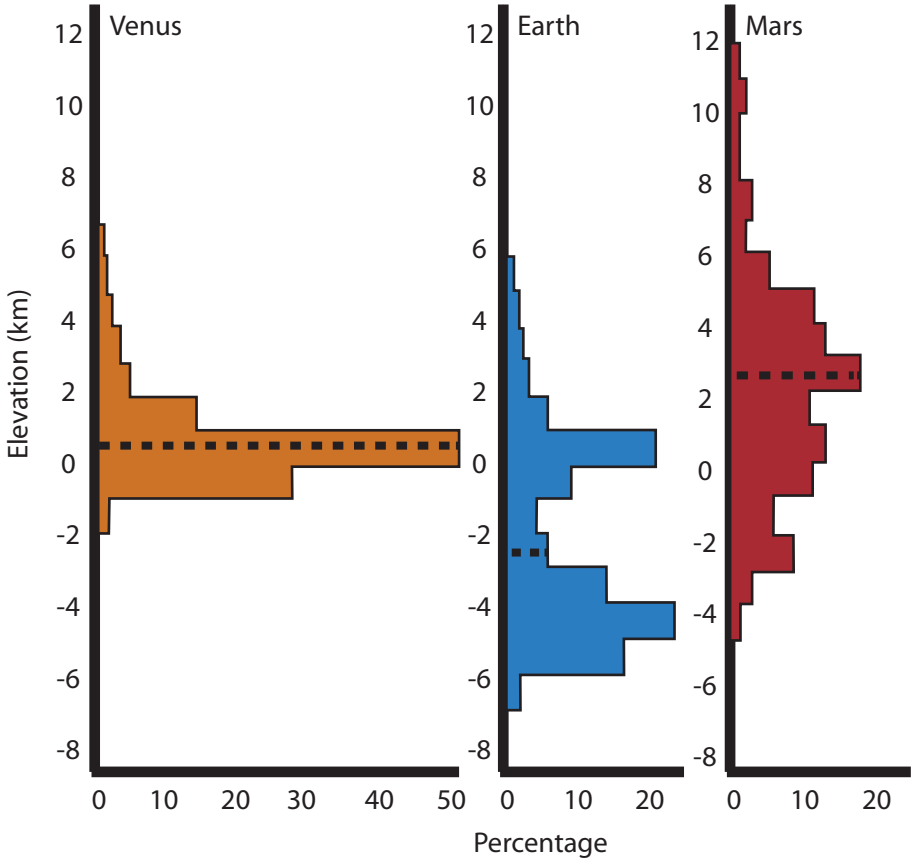

Fig. 1. Hypsography of Venus, Earth, and Mars (Head and Solomon, 1981; Basilevsky and Head, 2003; Taylor and McLennan, 2009). Dashed lines mark the mean surface relief for each planet.

1996). To wit, Earth's ocean basins are not littered with coronae, but with well-formed stratovolcanoes (i.e., seamounts).

The principal goal of this contribution is to explore the reasons as to why Earth hosts vastly more intraplate volcanoes than Venus. To do so, we formulate a conceptual model that combines data from rock deformation experiments on basalts, which inform on the mechanical behaviour of the crust and therefore the depth of the brittle-ductile transition (BDT) on both planets, with atmospheric noble gas isotope data from Earth and Venus, which inform on planetary volcanic flux. Additionally, our model also offers an explanation as to why volcanoes on Venus are morphologically distinct from those on Earth.

2. The deformation mode of the Terran and Venusian crusts

The depth of the BDT on Venus has been estimated numerous times. For example, first-order morphological differences between fold and thrust belts on Earth and Venus can be explained by a shallow BDT on Venus relative to Earth (Williams et al., 1994). Spacing between adjacent extensional structures may match the spacing between linear bands seen in the mountains of Ishtar Terra on Venus if the surficial brittle layer is no more than a few km in thickness (Solomon and Head, 1984). Preservation of substantial crater topographic relief on Venus is likely the result of a thin (<10 km) brittle crust (Grimm and Solomon, 1988). Further, surface features within tesserae (e.g., ribbons, long-wavelength folds, and grabens) offer a wealth of information as to the depth and evolution of the BDT on Venus (Phillips and Hanson, 1998). For example, ribbons within tesserae (Hansen and Willis, 1996) suggest a BDT as shallow as ~1 km during their formation (Hansen and Willis, 1998; Ghent and Hansen, 1999; Ruiz, 2007). Of interest, long-wavelength folds and graben are thought to reflect a deepening of the BDT over time (Phillips and Hanson, 1998)—but the depth of the BDT during the formation of long-wavelength folds is estimated at only ~6 km depth (Brown and Grimm, 1997; Ghent and Hansen, 1999). The pervasive deformation of the plateau highland tesserae, the oldest preserved terrain, requires a weak, thin lithosphere (Brown and Grimm, 1999). However, the presence of highland regions and large shield volcanoes (e.g., Crumpler et al., 1986; Smrekar and Solomon, 1992; McGovern et al., 2014) implies localised crustal domains where the BDT is deep enough to provide support for these structures. Nonetheless, these studies suggest that, on average, the BDT on Venus is shallow (and certainly much more than on Earth).

We use here an experimental rock deformation approach to provide an alternate assessment for the depth of the present-day BDT on Venus and Earth (see also Heap et al., 2017a), which we interpret here as a purely mechanical boundary between brittle and ductile behaviour. To do so, we compiled experimental rock deformation data on basaltic (and diabase) samples deformed over a range of confining pressures (analogous to depth) and temperatures (Table 1). We used these data to construct a failure mode map that highlights the pressures and temperatures at which basaltic (and diabase) rocks behave either in a brittle or a ductile manner in response to applied stress. We then used this map to assess the position (depth) of the BDT on Earth and Venus. We first review some important considerations for our experimental approach.

2.1. Considerations for our experimental approach

2.1.1. Composition of the Venusian crust

There is a dearth of *in-situ* quantitative geochemical data for Venusian surface rocks, and the planet's thick CO_2-dominated atmosphere makes optical geological observations from orbit or Earth-based telescopes impossible. The only available *in-situ* geochemical data from Venus are the major element composition of surface rocks, measured using gamma-ray and X-ray fluorescence spectroscopy. The three localities measured show basaltic compositions with SiO_2, FeO, MnO, and MgO abundances similar to mid-ocean ridge basalts on Earth (summarised in Bougher et al., 1997). Furthermore, the data from Venera 13 and 14 (Fe/Mg, Mg/Mn, K/U, and U/Th ratios) suggest Venus and Earth are made of the same chondritic material and have a similar internal structure, and that Venusian basalts are the product of similar degrees of partial (peridotite) mantle melting as those on Earth (Treiman, 2007; Hess and Head, 1990). Combined with the geomorphological data of Venus from radar imagery (i.e., reflectance spectra), it appears that most of the Venusian surface is volcanic in origin. This means the vast majority of the Venusian and Terran crusts are basaltic in their bulk composition (Basilevsky and Head, 2003). Therefore, we consider the deformation mode (i.e., brittle or ductile) of basaltic rocks collected on Earth to be analogous to the deformation mode of those on Venus.

2.1.2. Hydration of the Venusian crust

The Venusian atmosphere is extremely arid, with 150 times less H_2O compared with Earth's exosphere (Donahue and Russell, 1997). However, the lack of water in Venus' atmosphere and on its surface does not necessarily imply a desiccated crust. We suggest that the degree of hydration for Venusian crust and mantle (e.g., Kaula, 1990; Nimmo and McKenzie, 1996; Mackwell et al., 1998) requires re-examination. Note that the degassing of water is extremely inefficient for one-plate planets such as Venus or Mars. For example, it has been modelled that 90–95% of Mars' primordial water reserves should be retained in the mantle following accretion (Hunten, 1993), and recent data show the Martian mantle to be as 'wet' as the Terran mantle (McCubbin et al., 2012).

Combined, these studies conclude that substantial aqueous fluids can remain within planetary interiors, irrespective of the plate tectonic regime and without correlation to the degree of surface desiccation. For instance, if one were to distribute all of the water in the Earth's oceans into the Venusian mantle, the water abundance (distributed in nominally anhydrous minerals) would not exceed the storage capacity of a peridotitic mantle (Bell and Rossman, 1992; Kohlstedt et al., 1996; Bolfan-Casanova et al., 2000; Lécuyer et al., 2010; Hirschmann, 2006; Smyth et al., 2006). Furthermore, the Martian surface and atmosphere are both very water poor, but we know that the crust on Mars is hydrated (Carr and Head, 2010, 2015). A volatile-rich interior on Venus (or at least a hydrated mantle) could result in explosive volcanism (Thornhill, 1993; Fagents and Wilson, 1995; Glaze et al., 2011; Airey et al., 2015), and some workers have proposed that some morphological units on the Venusian surface are pyroclastic deposits (Campbell and Rogers, 1994; McGill, 2000; Grosfils et al., 2011; Ghail and Wilson, 2013). Therefore, it is difficult to definitively conclude whether the crust and upper mantle on Venus is desiccated or hydrous, and only future missions to Venus can resolve this question. Because of this ambiguity, we contend that the consideration of all of the available experimental rock deformation data for basalt and diabase (including the ultra-dry diabase data from Mackwell et al., 1998) is an effective approach to investigate the failure mode of rock within the Venusian crust. We also note that the majority of the basalts deformed in these studies only contain a subordinate glass phase, if any. As a result, the impact of a glass phase, hydrated or otherwise, should only play a very minor role in dictating the rheological behaviour of a given sample (Smith et al., 2011; Violay et al., 2012, 2015).

Table 1
Summary of the experimental conditions for the rock deformation experiments used in this study (for the construction of Figs. 3 and 4) (see also Heap et al., 2017a). *Pc* = confining pressure; *Pp* = pore fluid pressure; *Peff* = effective pressure; *T* = experimental temperature; σ_p = peak differential stress (see Fig. 2). In some cases, failure mode classification differs from that stated in the original publication. Data not included in this compilation are uniaxial experiments conducted at room temperature and instances of non-viscous ductile deformation (see text for details).

Reference	*Pc* (MPa)	*Pp* (MPa)	*Peff* (MPa)	*T* (°C)	σ_p (MPa)	Failure mode	Notes
Griggs et al. (1960)	500	0	500	25	1668	Brittle	Basalt
Griggs et al. (1960)	500	0	500	300	1390	Brittle	Basalt
Griggs et al. (1960)	500	0	500	500	1080	Brittle	Basalt
Griggs et al. (1960)	500	0	500	700	–	Ductile	Basalt
Griggs et al. (1960)	500	0	500	800	–	Ductile	Basalt
Caristan (1982)	0	0	0	950	199	Brittle	Maryland diabase; strain rate = 10^{-3} s^{-1}
Caristan (1982)	0	0	0	970	223	Brittle	Maryland diabase; strain rate = 10^{-5} s^{-1}
Caristan (1982)	0	0	0	995	193	Brittle	Maryland diabase; strain rate = 10^{-3} s^{-1}
Caristan (1982)	30	0	30	1000	370	Brittle	Maryland diabase; strain rate = 10^{-3} s^{-1}
Caristan (1982)	50	0	50	1000	440	Brittle	Maryland diabase; strain rate = 10^{-3} s^{-1}
Caristan (1982)	150	0	150	810	780	Brittle	Maryland diabase; strain rate = 10^{-6} s^{-1}
Caristan (1982)	150	0	150	970	385	Brittle	Maryland diabase; strain rate = 10^{-6} s^{-1}
Caristan (1982)	150	0	150	994	535	Brittle	Maryland diabase; strain rate = 10^{-3} s^{-1}
Caristan (1982)	150	0	150	1000	566	Brittle	Maryland diabase; strain rate = 10^{-4} s^{-1}
Caristan (1982)	150	0	150	1000	561	Brittle	Maryland diabase; strain rate = 10^{-5} s^{-1}
Caristan (1982)	150	0	150	1000	573	Brittle	Maryland diabase; strain rate = 10^{-5} s^{-1}
Caristan (1982)	350	0	350	1000	–	Ductile	Maryland diabase; strain rate = 10^{-5} s^{-1}
Caristan (1982)	400	0	400	1000	–	Ductile	Maryland diabase; strain rate = 10^{-4} s^{-1}
Caristan (1982)	425	0	425	1000	–	Ductile	Maryland diabase; strain rate = 10^{-4} s^{-1}
Caristan (1982)	425	0	425	1000	–	Ductile	Maryland diabase; strain rate = 10^{-5} s^{-1}
Caristan (1982)	425	0	425	1000	–	Ductile	Maryland diabase; strain rate = 10^{-6} s^{-1}
Caristan (1982)	450	0	450	1000	–	Ductile	Maryland diabase; strain rate = 10^{-5} s^{-1}
Shimada and Yukutake (1982)	57	0	57	25	400	Brittle	Yakuno basalt; Porosity = 0.07; strain rate = 10^{-5} s^{-1}
Shimada and Yukutake (1982)	107	0	107	25	415	Brittle	Yakuno basalt; Porosity = 0.07; strain rate = 10^{-5} s^{-1}
Bauer et al. (1981)	50	0	50	25	540	Brittle	Cuerbio basalt; Porosity = 0.05–0.08; strain rate = 10^{-4} s^{-1}
Bauer et al. (1981)	50	0	50	25	400	Brittle	Cuerbio basalt; Porosity = 0.05–0.08; strain rate = 10^{-4} s^{-1}
Bauer et al. (1981)	50	0	50	600	300	Brittle	Cuerbio basalt; Porosity = 0.05–0.08; strain rate = 10^{-4} s^{-1}
Bauer et al. (1981)	50	0	50	600	340	Brittle	Cuerbio basalt; Porosity = 0.05–0.08; strain rate = 10^{-4} s^{-1}
Bauer et al. (1981)	50	0	50	700	300	Brittle	Cuerbio basalt; Porosity = 0.05–0.08; strain rate = 10^{-4} s^{-1}
Bauer et al. (1981)	50	0	50	940	125	Brittle	Cuerbio basalt; Porosity = 0.05–0.08; strain rate = 10^{-4} s^{-1}
Bauer et al. (1981)	50	0	50	940	200	Brittle	Cuerbio basalt; Porosity = 0.05–0.08; strain rate = 10^{-4} s^{-1}
Bauer et al. (1981)	50	0	50	1000	100	Brittle	Cuerbio basalt; Porosity = 0.05–0.08; strain rate = 10^{-4} s^{-1}
Bauer et al. (1981)	100	0	100	700	465	Brittle	Cuerbio basalt; Porosity = 0.05–0.08; strain rate = 10^{-4} s^{-1}
Bauer et al. (1981)	100	0	100	900	240	Brittle	Cuerbio basalt; Porosity = 0.05–0.08; strain rate = 10^{-4} s^{-1}
Bauer et al. (1981)	100	0	100	950	110	Brittle	Cuerbio basalt; Porosity = 0.05–0.08; strain rate = 10^{-4} s^{-1}
Bauer et al. (1981)	100	0	100	1000	180	Brittle	Cuerbio basalt; Porosity = 0.05–0.08; strain rate = 10^{-4} s^{-1}
Bauer et al. (1981)	100	50	50	820	180	Brittle	Cuerbio basalt; Porosity = 0.05–0.08; strain rate = 10^{-4} s^{-1}
Shimada (1986)	57	0	57	25	410	Brittle	Yakuno basalt; Porosity = 0.07; strain rate = 10^{-5} s^{-1}
Duclos and Paquet (1991)	0	0	0	300	399	Brittle	Alkaline basalt; partially glassy; strain rate = 10^{-6} s^{-1}
Duclos and Paquet (1991)	0	0	0	600	430	Brittle	Alkaline basalt; partially glassy; strain rate = 10^{-6} s^{-1}
Duclos and Paquet (1991)	0	0	0	700	445	Brittle	Alkaline basalt; partially glassy; strain rate = 10^{-6} s^{-1}
Duclos and Paquet (1991)	0	0	0	750	430	Brittle	Alkaline basalt; partially glassy; strain rate = 10^{-6} s^{-1}
Duclos and Paquet (1991)	0	0	0	800	–	Ductile	Alkaline basalt; partially glassy; strain rate = 10^{-6} s^{-1}
Duclos and Paquet (1991)	0	0	0	900	–	Ductile	Alkaline basalt; partially glassy; strain rate = 10^{-6} s^{-1}
Duclos and Paquet (1991)	0	0	0	1000	–	Ductile	Alkaline basalt; partially glassy; strain rate = 10^{-6} s^{-1}
Hacker and Christie (1991)	1000	0	1000	675	–	Ductile	Tholeiitic basalt; partially glassy; 0.5 wt.% water added; strain rate = 10^{-4}–10^{-7} s^{-1}
Hacker and Christie (1991)	1000	0	1000	725	–	Ductile	Tholeiitic basalt; partially glassy; 0.5 wt.% water added; strain rate = 10^{-4}–10^{-7} s^{-1}
Hacker and Christie (1991)	1000	0	1000	775	–	Ductile	Tholeiitic basalt; partially glassy; 0.5 wt.% water added; strain rate = 10^{-4}–10^{-7} s^{-1}
Hacker and Christie (1991)	1000	0	1000	825	–	Ductile	Tholeiitic basalt; partially glassy; 0.5 wt.% water added; strain rate = 10^{-4}–10^{-7} s^{-1}
Hacker and Christie (1991)	1000	0	1000	875	–	Ductile	Tholeiitic basalt; partially glassy; 0.5 wt.% water added; strain rate = 10^{-4}–10^{-7} s^{-1}
Schultz (1993)	0	0	0	450	210	Brittle	Estimated strength value taken as 80% of the average uniaxial compressive strength for basalt; see Schultz (1993) for details
Mackwell et al. (1998)	400	0	400	1000	–	Ductile	Dehydrated Maryland and Columbia diabase; creep test; strain rate = 10^{-5}–10^{-7} s^{-1}

(*continued on next page*)

Table 1 (*continued*)

Reference	*Pc* (MPa)	*Pp* (MPa)	*Peff* (MPa)	*T* (°C)	σ_p (MPa)	Failure mode	Notes
Mackwell et al. (1998)	400	0	400	1050	–	Ductile	Dehydrated Maryland and Columbia diabase; creep test; strain rate = 10^{-5}–10^{-7} s^{-1}
Mackwell et al. (1998)	400	0	400	1050	–	Ductile	Dehydrated Maryland and Columbia diabase; creep test; strain rate = 10^{-5}–10^{-7} s^{-1}
Mackwell et al. (1998)	450	0	450	970	–	Ductile	Dehydrated Maryland and Columbia diabase; creep test; strain rate = 10^{-5}–10^{-7} s^{-1}
Mackwell et al. (1998)	450	0	450	1000	–	Ductile	Dehydrated Maryland and Columbia diabase; creep test; strain rate = 10^{-5}–10^{-7} s^{-1}
Mackwell et al. (1998)	450	0	450	1050	–	Ductile	Dehydrated Maryland and Columbia diabase; creep test; strain rate = 10^{-5}–10^{-7} s^{-1}
Mackwell et al. (1998)	500	0	500	1000	–	Ductile	Dehydrated Maryland and Columbia diabase; creep test; strain rate = 10^{-5}–10^{-7} s^{-1}
Rocchi et al. (2004)	0	0	0	300	89	Brittle	Vesuvius basalt; Porosity = 0.08–0.10; strain rate = 10^{-5} s^{-1}
Rocchi et al. (2004)	0	0	0	300	104	Brittle	Etna "core" basalt; strain rate = 10^{-5} s^{-1}
Rocchi et al. (2004)	0	0	0	300	35	Brittle	Etna "crust" basalt; strain rate = 10^{-5} s^{-1}
Rocchi et al. (2004)	0	0	0	600	96	Brittle	Vesuvius basalt; Porosity = 0.08–0.10; strain rate = 10^{-5} s^{-1}
Rocchi et al. (2004)	0	0	0	600	105	Brittle	Vesuvius basalt; Porosity = 0.08–0.10; strain rate = 10^{-5} s^{-1}
Rocchi et al. (2004)	0	0	0	600	103	Brittle	Etna "core" basalt; strain rate = 10^{-5} s^{-1}
Rocchi et al. (2004)	0	0	0	600	181	Brittle	Etna "core" basalt; strain rate = 10^{-5} s^{-1}
Rocchi et al. (2004)	0	0	0	600	40.5	Brittle	Etna "crust" basalt; strain rate = 10^{-5} s^{-1}
Rocchi et al. (2004)	0	0	0	700	33	Brittle	Etna "crust" basalt; strain rate = 10^{-5} s^{-1}
Rocchi et al. (2004)	0	0	0	800	42	Brittle	Vesuvius basalt; Porosity = 0.08–0.10; strain rate = 10^{-5} s^{-1}
Rocchi et al. (2004)	0	0	0	800	43	Brittle	Etna "core" basalt; strain rate = 10^{-4} s^{-1}
Rocchi et al. (2004)	0	0	0	800	25	Brittle	Etna "core" basalt; strain rate = 10^{-5} s^{-1}
Rocchi et al. (2004)	0	0	0	800	17	Brittle	Etna "core" basalt; strain rate = 10^{-6} s^{-1}
Rocchi et al. (2004)	0	0	0	800	20	Brittle	Etna "crust" basalt; strain rate = 10^{-4} s^{-1}
Rocchi et al. (2004)	0	0	0	900	50	Brittle	Vesuvius basalt; Porosity = 0.08–0.10; strain rate = 10^{-4} s^{-1}
Rocchi et al. (2004)	0	0	0	900	38	Brittle	Vesuvius basalt; Porosity = 0.08–0.10; strain rate = 10^{-5} s^{-1}
Rocchi et al. (2004)	0	0	0	900	29	Brittle	Vesuvius basalt; Porosity = 0.08–0.10; strain rate = 10^{-5} s^{-1}
Rocchi et al. (2004)	0	0	0	900	31	Brittle	Vesuvius basalt; Porosity = 0.08–0.10; strain rate = 10^{-6} s^{-1}
Rocchi et al. (2004)	5	0	5	25	108	Brittle	Vesuvius basalt; Porosity = 0.08–0.10; strain rate = 10^{-5} s^{-1}
Rocchi et al. (2004)	10	0	10	25	104	Brittle	Vesuvius basalt; Porosity = 0.08–0.10; strain rate = 10^{-5} s^{-1}
Rocchi et al. (2004)	10	0	10	300	101	Brittle	Vesuvius basalt; Porosity = 0.08–0.10; strain rate = 10^{-5} s^{-1}
Rocchi et al. (2004)	10	0	10	300	88	Brittle	Vesuvius basalt; Porosity = 0.08–0.10; strain rate = 10^{-5} s^{-1}
Rocchi et al. (2004)	10	0	10	600	116	Brittle	Vesuvius basalt; Porosity = 0.08–0.10; strain rate = 10^{-5} s^{-1}
Rocchi et al. (2004)	10	0	10	916	62	Brittle	Vesuvius basalt; Porosity = 0.08–0.10; strain rate = 10^{-5} s^{-1}
Rocchi et al. (2004)	12	0	12	25	93	Brittle	Vesuvius basalt; Porosity = 0.08–0.10; strain rate = 10^{-5} s^{-1}
Rocchi et al. (2004)	15	0	15	25	101	Brittle	Vesuvius basalt; Porosity = 0.08–0.10; strain rate = 10^{-5} s^{-1}
Rocchi et al. (2004)	17	0	17	25	100	Brittle	Vesuvius basalt; Porosity = 0.08–0.10; strain rate = 10^{-5} s^{-1}
Rocchi et al. (2004)	20	0	20	25	109	Brittle	Vesuvius basalt; Porosity = 0.08–0.10; strain rate = 10^{-5} s^{-1}
Rocchi et al. (2004)	20	0	20	300	95	Brittle	Vesuvius basalt; Porosity = 0.08–0.10; strain rate = 10^{-5} s^{-1}
Rocchi et al. (2004)	20	0	20	300	91	Brittle	Vesuvius basalt; Porosity = 0.08–0.10; strain rate = 10^{-5} s^{-1}
Rocchi et al. (2004)	20	0	20	600	118	Brittle	Vesuvius basalt; Porosity = 0.08–0.10; strain rate = 10^{-5} s^{-1}
Rocchi et al. (2004)	30	0	30	25	112	Brittle	Vesuvius basalt; Porosity = 0.08–0.10; strain rate = 10^{-5} s^{-1}
Rocchi et al. (2004)	30	0	30	25	103	Brittle	Vesuvius basalt; Porosity = 0.08–0.10; strain rate = 10^{-5} s^{-1}
Rocchi et al. (2004)	30	0	30	300	105	Brittle	Vesuvius basalt; Porosity = 0.08–0.10; strain rate = 10^{-5} s^{-1}
Rocchi et al. (2004)	30	0	30	300	87	Brittle	Vesuvius basalt; Porosity = 0.08–0.10; strain rate = 10^{-5} s^{-1}
Rocchi et al. (2004)	30	0	30	600	104	Brittle	Vesuvius basalt; Porosity = 0.08–0.10; strain rate = 10^{-5} s^{-1}
Rocchi et al. (2004)	30	0	30	604	79	Brittle	Vesuvius basalt; Porosity = 0.08–0.10; strain rate = 10^{-5} s^{-1}
Rocchi et al. (2004)	0	0	0	900	–	Ductile	Etna "crust" basalt; strain rate = 10^{-5} s^{-1}
Rocchi et al. (2004)	0	0	0	912	–	Ductile	Etna "core" basalt; strain rate = 10^{-5} s^{-1}
Rocchi et al. (2004)	0	0	0	1001	–	Ductile	Vesuvius basalt; Porosity = 0.08–0.10; strain rate = 10^{-5} s^{-1}
Apuani et al. (2005)	4	0	4	25	98	Brittle	Vigna Vecchia basalt (Stromboli)
Apuani et al. (2005)	4	0	4	25	72	Brittle	Vigna Vecchia basalt (Stromboli)
Apuani et al. (2005)	4	0	4	25	67	Brittle	Vigna Vecchia basalt (Stromboli)
Apuani et al. (2005)	8	0	8	25	88	Brittle	Vigna Vecchia basalt (Stromboli)
Apuani et al. (2005)	8	0	8	25	99	Brittle	Vigna Vecchia basalt (Stromboli)
Apuani et al. (2005)	12	0	12	25	104	Brittle	Vigna Vecchia basalt (Stromboli)
Apuani et al. (2005)	12	0	12	25	109	Brittle	Vigna Vecchia basalt (Stromboli)
Apuani et al. (2005)	16	0	16	25	54	Brittle	Vigna Vecchia basalt (Stromboli)
Apuani et al. (2005)	16	0	16	25	62	Brittle	Vigna Vecchia basalt (Stromboli)
Apuani et al. (2005)	16	0	16	25	87	Brittle	Vigna Vecchia basalt (Stromboli)

Apuani et al. (2005)	16	0	16	25	94	Brittle	Vigna Vecchia basalt (Stromboli)
Apuani et al. (2005)	20	0	20	25	56	Brittle	Vigna Vecchia basalt (Stromboli)
Apuani et al. (2005)	20	0	20	25	109	Brittle	Vigna Vecchia basalt (Stromboli)
Apuani et al. (2005)	20	0	20	25	178	Brittle	Vigna Vecchia basalt (Stromboli)
Benson et al. (2007)	60	20	40	25	475	Brittle	Etna basalt; porosity = 0.04; strain rate = 10^{-6} s^{-1}
Ougier-Simonin et al. (2011)	15	0	15	25	370	Brittle	Seljadur basalt; porosity = 0.05; strain rate = 10^{-6} s^{-1}
Heap et al. (2011)	30	20	10	25	291	Brittle	Etna basalt; porosity = 0.4; strain rate = 10^{-5} s^{-1}
Heap et al. (2011)	50	20	30	25	287	Brittle	Etna basalt; porosity = 0.4; strain rate = 10^{-5} s^{-1}
Heap et al. (2011)	70	20	50	25	504	Brittle	Etna basalt; porosity = 0.4; strain rate = 10^{-5} s^{-1}
Heap et al. (2011)	50	20	30	25	375	Brittle	Etna basalt; porosity = 0.4; creep test; strain rate = 10^{-6} s^{-1}
Heap et al. (2011)	50	20	30	25	357	Brittle	Etna basalt; porosity = 0.4; creep test; strain rate = 10^{-7} s^{-1}
Heap et al. (2011)	50	20	30	25	329	Brittle	Etna basalt; porosity = 0.4; creep test; strain rate = 10^{-8} s^{-1}
Heap et al. (2011)	50	20	30	25	304	Brittle	Etna basalt; porosity = 0.4; creep test; strain rate = 10^{-9} s^{-1}
Violay et al. (2012)	100	0	100	400	1002	Brittle	Aphanitic basalt; porosity = 0.02; strain rate = 10^{-5} s^{-1}
Violay et al. (2012)	100	0	100	400	902	Brittle	Porphyritic basalt; partially glassy; porosity = 0.02; strain rate = 10^{-5} s^{-1}
Violay et al. (2012)	100	0	100	600	854	Brittle	Aphanitic basalt; porosity = 0.02; strain rate = 10^{-5} s^{-1}
Violay et al. (2012)	100	0	100	700	508	Brittle	Aphanitic basalt; porosity = 0.02; strain rate = 10^{-5} s^{-1}
Violay et al. (2012)	100	0	100	800	462	Brittle	Aphanitic basalt; porosity = 0.02; strain rate = 10^{-5} s^{-1}
Violay et al. (2012)	100	0	100	800	446	Brittle	Aphanitic basalt; porosity = 0.02; strain rate = 10^{-5} s^{-1}
Violay et al. (2012)	100	0	100	900	355	Brittle	Aphanitic basalt; porosity = 0.02; strain rate = 10^{-5} s^{-1}
Violay et al. (2012)	300	0	300	600	749	Brittle	Aphanitic basalt; porosity = 0.02; strain rate = 10^{-5} s^{-1}
Violay et al. (2012)	300	0	300	700	755	Brittle	Aphanitic basalt; porosity = 0.02; strain rate = 10^{-5} s^{-1}
Violay et al. (2012)	300	0	300	800	518	Brittle	Aphanitic basalt; porosity = 0.02; strain rate = 10^{-5} s^{-1}
Violay et al. (2012)	50	0	50	600	–	Ductile	Porphyritic basalt; partially glassy; porosity = 0.02; strain rate = 10^{-5} s^{-1}
Violay et al. (2012)	70	0	70	600	–	Ductile	Porphyritic basalt; partially glassy; porosity = 0.02; strain rate = 10^{-5} s^{-1}
Violay et al. (2012)	100	0	100	500	–	Ductile	Porphyritic basalt; partially glassy; porosity = 0.02; strain rate = 10^{-5} s^{-1}
Violay et al. (2012)	100	0	100	600	–	Ductile	Porphyritic basalt; partially glassy; porosity = 0.02; strain rate = 10^{-5} s^{-1}
Violay et al. (2012)	100	0	100	600	–	Ductile	Porphyritic basalt; partially glassy; porosity = 0.02; strain rate = 10^{-5} s^{-1}
Violay et al. (2012)	100	0	100	700	–	Ductile	Porphyritic basalt; partially glassy; porosity = 0.02; strain rate = 10^{-5} s^{-1}
Violay et al. (2012)	100	0	100	800	–	Ductile	Porphyritic basalt; partially glassy; porosity = 0.02; strain rate = 10^{-5} s^{-1}
Violay et al. (2012)	100	0	100	800	–	Ductile	Porphyritic basalt; partially glassy; porosity = 0.02; strain rate = 10^{-5} s^{-1}
Violay et al. (2012)	100	0	100	800	–	Ductile	Porphyritic basalt; partially glassy; porosity = 0.02; strain rate = 10^{-5} s^{-1}
Violay et al. (2012)	100	0	100	900	–	Ductile	Porphyritic basalt; partially glassy; porosity = 0.02; strain rate = 10^{-5} s^{-1}
Violay et al. (2012)	100	0	100	900	–	Ductile	Porphyritic basalt; partially glassy; porosity = 0.02; strain rate = 10^{-5} s^{-1}
Violay et al. (2012)	100	0	100	900	–	Ductile	Porphyritic basalt; partially glassy; porosity = 0.02; strain rate = 10^{-5} s^{-1}
Violay et al. (2012)	250	0	250	650	–	Ductile	Porphyritic basalt; partially glassy; porosity = 0.02; strain rate = 10^{-5} s^{-1}
Violay et al. (2012)	300	0	300	600	–	Ductile	Porphyritic basalt; partially glassy; porosity = 0.02; strain rate = 10^{-5} s^{-1}
Violay et al. (2012)	300	0	300	700	–	Ductile	Porphyritic basalt; partially glassy; porosity = 0.02; strain rate = 10^{-5} s^{-1}
Violay et al. (2012)	300	0	300	750	–	Ductile	Porphyritic basalt; partially glassy; porosity = 0.02; strain rate = 10^{-5} s^{-1}
Violay et al. (2012)	300	0	300	800	–	Ductile	Porphyritic basalt; partially glassy; porosity = 0.02; strain rate = 10^{-5} s^{-1}
Violay et al. (2012)	300	0	300	800	–	Ductile	Aphanitic basalt; porosity = 0.02; strain rate = 10^{-5} s^{-1}
Violay et al. (2012)	300	0	300	850	–	Ductile	Aphanitic basalt; porosity = 0.02; strain rate = 10^{-5} s^{-1}
Violay et al. (2012)	300	0	300	900	–	Ductile	Aphanitic basalt; porosity = 0.02; strain rate = 10^{-5} s^{-1}
Violay et al. (2012)	300	0	300	900	–	Ductile	Porphyritic basalt; partially glassy; porosity = 0.02; strain rate = 10^{-5} s^{-1}
Violay et al. (2012)	300	0	300	950	–	Ductile	Aphanitic basalt; porosity = 0.02; strain rate = 10^{-5} s^{-1}
Adelinet et al. (2013)	10	5	5	25	120	Brittle	Reykjanes basalt; porosity = 0.08; strain rate = 10^{-6} s^{-1}
Adelinet et al. (2013)	80	76	4	25	118	Brittle	Reykjanes basalt; porosity = 0.08; strain rate = 10^{-6} s^{-1}
Violay et al. (2015)	130	30	100	600	877	Brittle	Aphanitic basalt; porosity = 0.03; strain rate = 10^{-5} s^{-1}
Violay et al. (2015)	130	30	100	650	834	Brittle	Aphanitic basalt; porosity = 0.03; strain rate = 10^{-5} s^{-1}
Violay et al. (2015)	130	30	100	700	792	Brittle	Aphanitic basalt; porosity = 0.03; strain rate = 10^{-5} s^{-1}
Violay et al. (2015)	130	30	100	750	699	Brittle	Aphanitic basalt; porosity = 0.03; strain rate = 10^{-5} s^{-1}
Violay et al. (2015)	130	30	100	800	717	Brittle	Aphanitic basalt; porosity = 0.03; strain rate = 10^{-5} s^{-1}
Violay et al. (2015)	130	30	100	900	382	Brittle	Aphanitic basalt; porosity = 0.03; strain rate = 10^{-5} s^{-1}
Violay et al. (2015)	130	30	100	1050	–	Ductile	Aphanitic basalt; porosity = 0.03; strain rate = 10^{-5} s^{-1}
Schaefer et al. (2015)	0	0	0	935	167	Brittle	Pacaya (Guatemala) basalt; porosity = 0.02; strain rate = 10^{-1} s^{-1}
Schaefer et al. (2015)	0	0	0	935	162	Brittle	Pacaya (Guatemala) basalt; porosity = 0.05; strain rate = 10^{-1} s^{-1}
Schaefer et al. (2015)	0	0	0	935	126	Brittle	Pacaya (Guatemala) basalt; porosity = 0.06; strain rate = 10^{-5} s^{-1}
Schaefer et al. (2015)	0	0	0	935	59	Brittle	Pacaya (Guatemala) basalt; porosity = 0.19; strain rate = 10^{-1} s^{-1}
Schaefer et al. (2015)	0	0	0	935	49	Brittle	Pacaya (Guatemala) basalt; porosity = 0.16; strain rate = 10^{-5} s^{-1}

(*continued on next page*)

Table 1 (*continued*)

Reference	*Pc* (MPa)	*Pp* (MPa)	*Peff* (MPa)	*T* (°C)	σ_p (MPa)	Failure mode	Notes
Schaeffer et al. 2015	0	0	0	935	93	Brittle	Pacaya (Guatemala) basalt; porosity = 0.19; strain rate = 10^{-1} s^{-1}
Schaefer et al. (2015)	0	0	0	935	44	Brittle	Pacaya (Guatemala) basalt; porosity = 0.19; strain rate = 10^{-5} s^{-1}
Schaefer et al. (2015)	0	0	0	935	75	Brittle	Pacaya (Guatemala) basalt; porosity = 0.23; strain rate = 10^{-1} s^{-1}
Schaefer et al. (2015)	0	0	0	935	64	Brittle	Pacaya (Guatemala) basalt; porosity = 0.21; strain rate = 10^{-5} s^{-1}
Schaefer et al. (2015)	0	0	0	935	28	Brittle	Pacaya (Guatemala) basalt; porosity = 0.32; strain rate = 10^{-1} s^{-1}
Schaefer et al. (2015)	0	0	0	935	16	Brittle	Pacaya (Guatemala) basalt; porosity = 0.31; strain rate = 10^{-5} s^{-1}
Zhu et al. (2016)	20	10	10	25	281	Brittle	Etna basalt (EB_I); porosity = 0.05; strain rate = 10^{-5} s^{-1}
Zhu et al. (2016)	20	10	10	25	240	Brittle	Etna basalt (EB_I); porosity = 0.05; strain rate = 10^{-5} s^{-1}
Zhu et al. (2016)	20	10	10	25	221	Brittle	Etna basalt (EB_I); porosity = 0.05; strain rate = 10^{-5} s^{-1}
Zhu et al. (2016)	20	10	10	25	327	Brittle	Etna basalt (EB_I); porosity = 0.05; strain rate = 10^{-5} s^{-1}
Zhu et al. (2016)	30	10	20	25	329	Brittle	Etna basalt (EB_I); porosity = 0.05; strain rate = 10^{-5} s^{-1}
Zhu et al. (2016)	30	10	20	25	361	Brittle	Etna basalt (EB_I); porosity = 0.05; strain rate = 10^{-5} s^{-1}
Zhu et al. (2016)	40	10	30	25	399	Brittle	Etna basalt (EB_I); porosity = 0.05; strain rate = 10^{-5} s^{-1}
Zhu et al. (2016)	50	10	40	25	403	Brittle	Etna basalt (EB_I); porosity = 0.05; strain rate = 10^{-5} s^{-1}
Zhu et al. (2016)	60	10	50	25	500	Brittle	Etna basalt (EB_I); porosity = 0.05; strain rate = 10^{-5} s^{-1}
Zhu et al. (2016)	60	10	50	25	493	Brittle	Etna basalt (EB_I); porosity = 0.05; strain rate = 10^{-5} s^{-1}
Zhu et al. (2016)	60	10	50	25	561	Brittle	Etna basalt (EB_I); porosity = 0.05; strain rate = 10^{-5} s^{-1}
Zhu et al. (2016)	80	10	70	25	563	Brittle	Etna basalt (EB_I); porosity = 0.05; strain rate = 10^{-5} s^{-1}
Zhu et al. (2016)	90	10	80	25	560	Brittle	Etna basalt (EB_I); porosity = 0.05; strain rate = 10^{-5} s^{-1}
Zhu et al. (2016)	90	10	80	25	574	Brittle	Etna basalt (EB_I); porosity = 0.05; strain rate = 10^{-5} s^{-1}
Zhu et al. (2016)	90	10	80	25	655	Brittle	Etna basalt (EB_I); porosity = 0.05; strain rate = 10^{-5} s^{-1}
Zhu et al. (2016)	110	10	100	25	658	Brittle	Etna basalt (EB_I); porosity = 0.04; strain rate = 10^{-5} s^{-1}
Zhu et al. (2016)	160	10	150	25	753	Brittle	Etna basalt (EB_I); porosity = 0.05; strain rate = 10^{-5} s^{-1}
Zhu et al. (2016)	60	10	50	25	365	Brittle	Etna basalt (EB_II); porosity = 0.08; strain rate = 10^{-5} s^{-1}
Zhu et al. (2016)	90	10	80	25	349	Brittle	Etna basalt (EB_II); porosity = 0.08; strain rate = 10^{-5} s^{-1}
Zhu et al. (2016)	20	10	10	25	224	Brittle	Etna basalt (EB_III); porosity = 0.05; strain rate = 10^{-5} s^{-1}
Zhu et al. (2016)	60	10	50	25	434	Brittle	Etna basalt (EB_III); porosity = 0.05; strain rate = 10^{-5} s^{-1}
Zhu et al. (2016)	90	10	80	25	543	Brittle	Etna basalt (EB_III); porosity = 0.05; strain rate = 10^{-5} s^{-1}
Zhu et al. (2016)	110	10	100	25	640	Brittle	Etna basalt (EB_III); porosity = 0.05; strain rate = 10^{-5} s^{-1}
Zhu et al. (2016)	160	10	150	25	798	Brittle	Etna basalt (EB_III); porosity = 0.05; strain rate = 10^{-5} s^{-1}

2.2. Determining the depth of the brittle–ductile transitions for Earth and Venus

2.2.1. Essential nomenclature: brittle and ductile

Before interpreting the collated experimental rock deformation data it is important to outline some essential nomenclature. The terms 'brittle' and 'ductile' are sometimes interpreted differently across disciplines, which can cause confusion. To avoid such confusion, we define how we use these terms.

Here, we use 'brittle' and 'ductile' to describe the failure mode of a rock sample on the lengthscale of that sample (typically between 10 and 100 mm). Brittle behaviour is characterised by localised deformation, typically manifest as axial splits or shear fractures. During a deformation experiment, it is typical to observe an increase in porosity of a sample as the peak stress is approached. This increase in porosity is the result of the growth and formation of dilatant microcracks. Following a peak stress, a brittle experiment involves a stress drop (i.e., strain softening). This stress drop marks the point at which a macroscopic (i.e., across the lengthscale of the sample) fracture is forming or has formed—the hallmark of a brittle failure mode (see Hoek and Bieniawski, 1965; Brace et al., 1966; Scholz, 1968). We note that, in the case of highly porous samples, brittle deformation can be associated with a net decrease in porosity. In these cases, inspection of the post-deformation sample is required to verify the presence of axial splits or shear fractures.

We use the term ductility as per the definition of Rutter (1986), who described it as simply the capacity of a material to accommodate qualitatively substantial strain without the tendency to localise the flow into faults—localisation does not occur on the sample lengthscale. The concept of ductility is not dependent on the mechanism of deformation (Rutter, 1986). Although brittle behaviour is always the result of cracking on the microscale, ductile behaviour can be the product of a number of micromechanisms. For example, the micromechanism behind low-temperature, high-pressure cataclastic flow (i.e., ductile behaviour) is microcracking (Menéndez et al., 1996; Wong et al., 1997). Ductile behaviour typically involves the loss of porosity. We note that ductile behaviour can be associated with strain localisation in certain circumstances: ductile behaviour in porous rocks can involve the formation of compaction bands (e.g., Baud et al., 2004) or bands of collapsed pores (e.g., Heap et al., 2015, Heap et al., 2017b). The formation of such features is also associated with small stress drops in the mechanical data. In ambiguous cases, inspection of the post-deformation sample is required to verify the absence of axial splits or shear fractures, features synonymous with a brittle failure mode. Mechanical behaviour for two experiments is shown in Fig. 2, a typical brittle test and a typical ductile test (Violay et al., 2012; Heap et al., 2017a).

2.2.2. Data selection

In the context of our study, we are interested in the transition between brittle behaviour and ductile behaviour as a result of viscous flow (i.e., the change in micromechanism from microcracking to viscous flow). We interpret viscous flow as non-recoverable viscoelastic deformation; this type of deformation is referred to as 'plastic' by some authors, but this term is sometimes also used to describe non-recoverable deformation in the brittle field. Since we are interested in the change in deformation micromechanism, we are not concerned here with low-temperature ductility driven by microcracking or cataclastic pore collapse, although very few studies exist on this topic for basaltic rocks (e.g., Shimada, 1986; Shimada et al., 1989; Adelinet et al., 2013; Zhu et al., 2016). We included all available experimental rock deformation data for basalt and diabase into our analysis (Table 1), with the exception of room-temperature experiments under uniaxial conditions (e.g., Al-Harthi et al., 1999; Heap et al., 2009; Schaefer et al., 2015), because they are of little use for determining the BDT, and those triaxial experiments that yielded non-viscous ductile behaviour such as cataclastic pore collapse (e.g., Shimada, 1986; Shimada et al., 1989; Adelinet et al., 2013; Zhu et al., 2016).

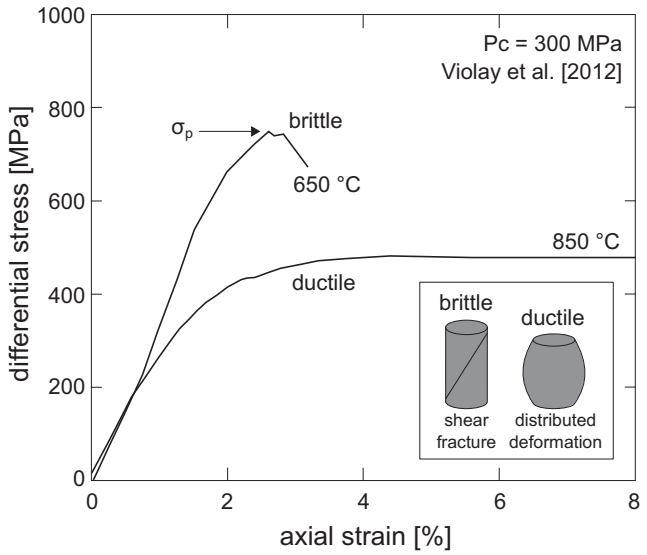

Fig. 2. The mechanical behaviour of rock in compression (from Heap et al., 2017a). Examples of brittle and ductile stress–strain curves for basalt deformed at a confining pressure of 300 MPa and a temperature of 650 °C (brittle test) and 850 °C (ductile test) (data from Violay et al., 2012). Inset shows cartoons depicting post-failure samples typical of brittle (thoroughgoing shear fracture) and ductile (distributed deformation) deformation.

2.2.3. Limitations to our approach

One obvious limitation of our collation approach is that typical laboratory strain rates ($\sim 10^{-5}$ s^{-1}) are much faster than tectonic strain rates (e.g., Grimm, 1994). However, we recognise that [1] experiments already classified as ductile at laboratory strain rates will remain ductile at lower (i.e., natural) strain rates, and [2] lowering the strain rate at low experimental pressures and temperatures will reduce rock strength—because of the increased time available for subcritical crack growth (see Brantut et al., 2013 for a review)—but may not promote ductile deformation *per se*. For example, the experiments of Heap et al. (2011) showed that basalt can still fail in a brittle manner at a low laboratory strain rate of 10^{-9} s^{-1}. Although our approach utilises experiments conducted at high strain rates, and so should be considered with this caveat in mind, our method does not assume a representative basalt for the Venusian crust (see Section 2.1 above).

2.2.4. Calculating depth

Each published experimental datum was assigned a failure mode: brittle or ductile, defined above. Where necessary, and when possible, our definitions supersede those outlined in the studies from which these data were collated. The effective pressure under which each experiment was performed were converted to a depth with the relation $P = \rho \cdot g \cdot h$, where P is lithospheric or hydrostatic pressure and g is surface gravitational acceleration taken as 9.807 and 8.87 m/s^2 for Earth and Venus, respectively. This approach allowed us to determine the lithostatic pressure gradients for Earth and Venus. The bulk rock density, ρ, was determined with the following relation (Wilson and Head, 1994):

$$\rho(h) = \frac{\rho_\infty}{[1 + \{V_0 - (1 - V_0)\} \exp(-\lambda \rho_\infty g z)]} \quad (1)$$

where ρ_∞ (the density of porosity-free rock) was taken as 2900 kg/m^3, V_0 is the void space fraction (i.e., total porosity) at the surface (assumed here to be 0.25; see Wilson and Head, 1994), and the constant λ was assumed to be 1.18×10^{-8} Pa^{-1} (Head and Wilson, 1992). Because of the very high atmospheric pressure of Venus, the lithostatic pressure at the surface was taken as 9 MPa. The hydrostatic pressure gradient for Earth was calculated using a constant water density of 1000 kg/m^3 (yielding a pore pressure gradient of ~9.8 MPa/km). We note that the density of water does not vary considerably at the pressures and temperatures relevant for the Earth's crust.

However, the nature of the pore fluid, and therefore the pore pressure gradient, for Venus is enigmatic. The behaviour of CO_2 at the atmospheric pressure and temperature of Venus is that of a supercritical fluid and, if one assumes that supercritical CO_2 is a plausible pore fluid for Venus, the density will vary with pressure and temperature. For example, the density of CO_2 at the surface of Venus (at a pressure of 9 MPa and a temperature of 460 °C) is 65 kg/m^3. CO_2 density increases to 457 kg/m^3 at a pressure of 100 MPa and a temperature of 600 °C. Because of the relatively broad parameter space for pore fluid behaviour (and composition) on Venus, we considered three scenarios that likely capture the range of possible pore fluid densities within the Venusian crust. In one, the pore fluid had a constant density of 1000 kg/m^3 (i.e., the same as on Earth, yielding a pore pressure gradient of ~8.9 MPa/km); in the second scenario, pore fluid had a density of 500 kg/m^3 and so a pore pressure gradient of ~4.4 MPa/km. In the third scenario, pore fluid density was 100 kg/m^3, giving a pore pressure gradient of ~0.89 MPa/km. In all cases, the pore pressure at the surface was taken as 9 MPa. In our analysis, we interpreted the pressure within the crust as the lithostatic pressure minus the pore fluid pressure.

2.2.5. Thermal gradients

Because we are discussing planetary-scale processes, we have opted to constrain the BDT on Earth using an average Terran geothermal gradient of 25 °C/km and an average surface temperature of 4 °C. Due to the lack of heat-flux measurements on Venus, all of the published thermal gradients are inferred. Importantly, as a result of the greenhouse effect imposed by an average atmospheric pressure of 9 MPa and a permanent cloud cover on Venus (Pollack et al., 1980), there is no meaningful difference in average surface temperature across the Venusian day–night cycle (where one Venusian day is equal to 116 Earth days) or with changes in latitude from the equator. In addition, since Venus has a hypsometry with a very low standard deviation (Fig. 1) there is an insignificant effect of altitude on the surface temperature when one considers a global average. Therefore, a representative surface temperature for Venus should have a small standard deviation from the assumed average value of 460 °C. To account for the uncertainty in the Venusian thermal gradient, we have used a selection of values from 5 to 40 °C/km (e.g., Sclater et al., 1980; Solomon and Head, 1982, 1984; Grimm and Solomon, 1988; Burt and Head, 1992; Turcotte, 1993, 1995; Solomatov and Moresi, 1996; Turcotte et al., 1999; Leitner and Firneis, 2006).

2.2.6. BDT estimates for Venus and Earth using experimental data

Once the effective pressure of each experiment was converted to a depth, these data were plotted against the experimental temperature to examine the predicted depth of the present-day brittle–ductile transition on Earth (Fig. 3) and Venus (Fig. 4). The majority of experiments performed with basaltic rock samples were conducted under pressures equating to depths from 0 km (i.e., the surface) to 7 km (Shimada and Yukutake, 1982; Caristan, 1982; Bauer and Handin, 1983; Shimada, 1986; Duclos and Paquet, 1991; Schultz, 1993; Rocchi et al., 2004; Apuani et al., 2005; Benson et al., 2007; Ougier-Simonin et al., 2011; Heap et al., 2011; Violay et al., 2012, 2015; Adelinet et al., 2013; Schaefer et al., 2015; Zhu et al., 2016); few studies were performed under pressures corresponding to depths of up to 40 km (Griggs et al., 1960; Caristan, 1982; Hacker and Christie, 1991; Mackwell et al., 1998; Violay et al., 2012, 2015). In all cases, ductile behaviour was not observed below temperatures of 500 °C, even under an effective pressure of 500 MPa (e.g., Griggs et al., 1960). As expected, ductile behaviour is more commonly observed under combined high pressure and high temperature. Surprisingly, ductile behaviour was observed under room pressure (i.e., 0.1 MPa) at 800 °C (Figs. 3 and 4), which was likely the result of the presence of a melt phase; therefore, although these samples were of a basaltic bulk composition, they may not typify basaltic rocks. However, we prefer to retain all data for rocks of a basaltic composition in our analysis, for two reasons: first, not all of the experimental studies offer a detailed microstructural and compositional breakdown of their basaltic samples; second, we do not want to remove data based on our interpretation of what constitutes a basaltic rock typical of Venus or Earth.

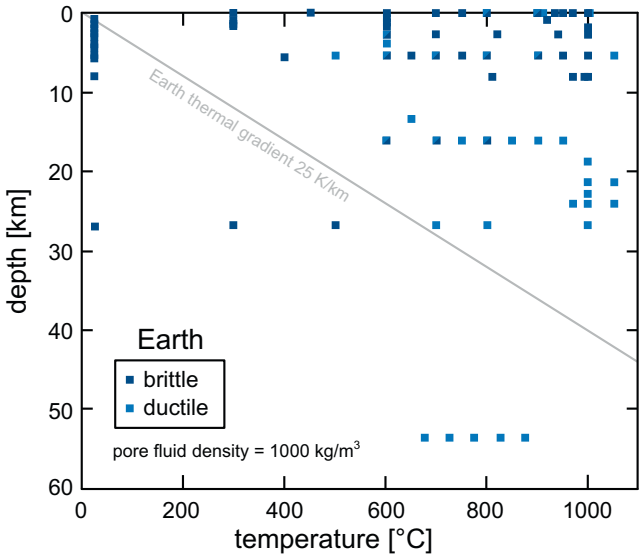

Fig. 3. Failure mode map (brittle or ductile) for Earth assuming a pore pressure gradient of ~ 9.8 MPa/km, a surface gravity of 9.807 m/s^2, an average thermal gradient of 25 °C/km, and an average surface temperature of 4 °C. See text for details.

Our analysis predicts that the BDT for the oceanic crust of Earth occurs at a depth of ~25–27 km (Fig. 3), consistent with the broad temperature-dependent (i.e., ~10–40 km depth) brittle–ductile transition predicted for a predominantly basaltic oceanic crust on Earth (Kohlstedt et al., 1995). Assuming a pore fluid pressure gradient on Venus of ~8.7 MPa/km (Fig. 4a), we find that most of the thermal gradients for Venus (i.e., 5–40 °C/km) pass through a zone (from ~5 to ~18 km depth) characterised by both brittle and ductile deformation. The difference in failure mode over this depth interval arises from differences in rock properties such as composition, crystal size and content, and porosity, as well as in factors such as strain rate (although we note that typically laboratory strain rates rarely deviate from 10^{-5} s^{-1}). We interpret this depth interval on Venus as a failure mode 'transitional' zone. Below a depth of ~20 km, our collated experimental data predict exclusively ductile behaviour when the thermal gradient is 15 °C/km or above for a pore pressure gradient of ~8.7 MPa/km (Fig. 4a). However, this failure mode transitional zone is much shallower in the (arguably more plausible) scenarios under which the Venusian pore pressure gradient is lower (Fig. 4b and c). The failure mode transition zone on Venus exists at a depth of ~4–14 km

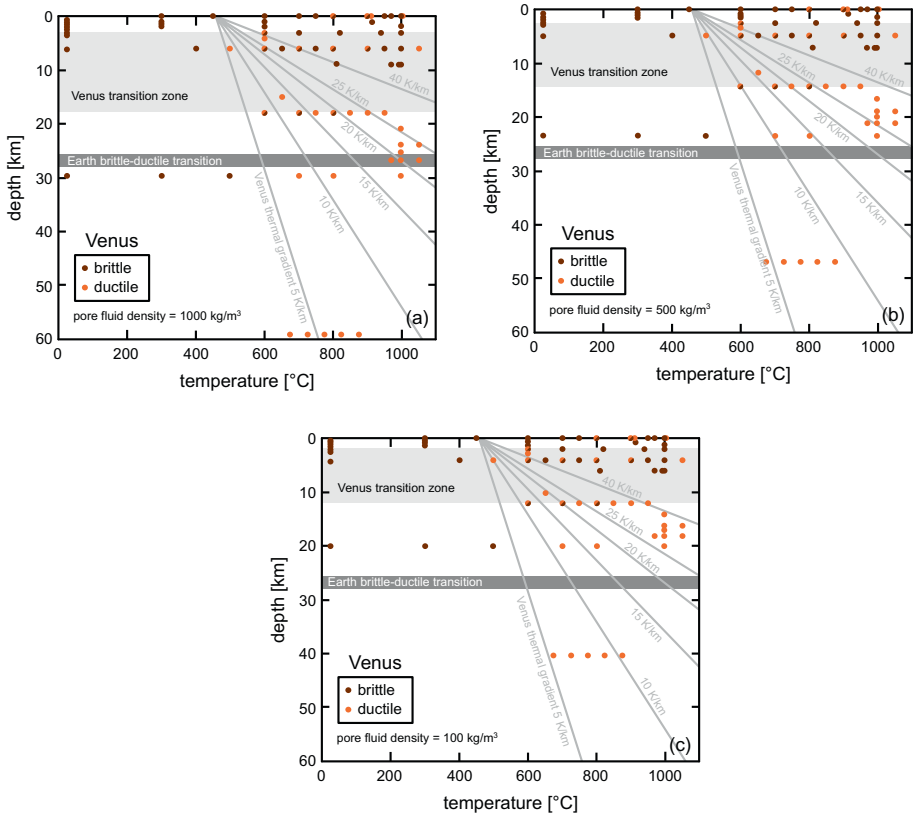

Fig. 4. Failure mode maps (brittle or ductile) for Venus assuming a surface gravity of 8.87 m/s^2 and an average surface temperature of 460 °C. Due to the uncertainty in the pore pressure gradient we provide three scenarios. (a) That the pore fluid has a constant density of 1000 kg/m^3 (i.e. the same as Earth; yielding a pore pressure gradient of ~ 8.9 MPa/km). (b) That the pore fluid has a constant density of 500 kg/m^3 (yielding a pore pressure gradient of ~ 4.4 MPa/km). (c) That the pore fluid has a constant density of 100 kg/m^3 (yielding a pore pressure gradient of ~ 0.89 MPa/km). Due to the uncertainty in the thermal gradient we provide a range from 5 to 40 °C/km. See text for details.

(Fig. 4b) or ~2–12 km (Fig. 4c) for pore pressure gradients of ~4.4 or ~0.89 MPa/km, respectively. If we assume a representative rock type for the Venusian crust and account for more realistic natural strain rates, published data show that the BDT for a "glassy" basalt and for a "non-glassy" basalt is ~100 °C and ~550 ± 100 °C, respectively (Violay et al., 2012). Therefore, if one considers an average surface temperature of 460 and 4 °C for Venus and Earth, respectively, then, assuming that the Terran and Venusian thermal gradients do not differ significantly, the BDT will always be shallower on Venus. Based on the data published in Violay et al. (2012), and using a thermal gradient of 25 °C/km), the BDT on Venus would be at the surface (a fact we know is not true, highlighting the uncertainties that can manifest when one assumes a representative rock type) or at a depth between 3 and 4 km, respectively. Improved estimates of the average depth of the BDT on Venus requires additional *in-situ* geological and geochemical data from the surface of Venus.

Based on these collated experimental data, we conclude that the BDT occurs at a substantially shallower depth on Venus than on Earth (when one considers global averages) (Figs. 3 and 4). Therefore, these data show that although much of the crust on Earth behaves in a brittle manner, the majority by volume of the Venusian crust should respond to stress in a ductile manner.

3. Implications of a dominantly ductile crust on Venus

3.1. Implications for volcano morphology

The tallest volcanoes on Earth, Venus, and Mars are intraplate volcanoes fed by deep-seated mantle plumes (Head and Solomon, 1981; Donahue and Russell, 1997; Herrick et al., 2005; Wilson, 2009): Mauna Loa on Earth (17.2 km of relief), Maat Mons on Venus (9 km of relief; Mouginis-Mark, 2016), and Olympus Mons on Mars (21.9 km of relief; Plescia, 2004), respectively). However, shield volcanoes on Earth and Venus are dramatically different in terms of morphology: those on Venus are, on average, wider and of lower relief than those on Earth (700 km wide and 1.5 km relief vs. 120 km wide and 8 km relief, respectively) (Head and Solomon, 1981; Head et al., 1992; Herrick et al., 2005; Wilson, 2009). Because the loci of intraplate volcanism on Earth vary as tectonic plates move across fixed mantle plumes, the maximum relief of a volcano is therefore not only supply limited, but is also constrained by the velocity of the plate (Morgan, 1971). By contrast, Venus' stagnant-lid tectonic regime enables a volcano to grow for as long as the magma source persists. Note, although it is debateable if plumes on Earth and Venus are geometrically similar (Schubert et al., 1990; Stofan et al., 1995; Smrekar and Stofan, 1997; Jellinek et al., 2002; Johnson and Richards, 2003; Ernst et al., 2007; Robin et al., 2007), the large shield volcanoes observed on the Venusian surface are taken as evidence for long-lived mantle plumes in the Venusian interior (Head and Solomon, 1981; Head et al., 1992; Herrick et al., 2005; Wilson, 2009). With all else being equal, the average relief of shield volcanoes on Venus should therefore be greater than their Terran counterparts (Wilson, 2009). But, other than some rare if notable exceptions (e.g., Maat and Skadi Montes), Venusian volcanoes are not higher in relief than their Terran counterparts. To explore this discrepancy we assess here three first-order variables that we consider important in controlling the relief of a volcanic construct: [1] surface gravity, [2] the viscosity of extruded lavas, and [3] the flexural response of the lithosphere to geological loads.

3.1.1. Surface gravity

Mars is host to the largest volcanoes in the Solar System. This is, in part, because high-relief structures are easier to build and retain on Mars because of its relatively low surface gravity (i.e., 3.71 m/s^2, compared with 9.81 m/s^2 and 8.81 m/s^2 on Earth and Venus, respectively) (Heap et al., 2017a). However, the surface gravitational acceleration on Venus is very similar to that of Earth meaning that, if all else were equal, both planets should extrude lava flows of a similar thickness and build shield volcanoes of a similar size over a given timescale. Large basaltic flows on Earth are typically <30 m thick, and—again, because of the comparable surface gravitational accelerations of Earth and Venus—the same should be true for Venus. This inference is consistent with radar imaging of Venus that shows that flows rarely exceed the vertical resolution of the Magellan topographic data (which has a height resolution of 5–50 m; e.g., Pettengill et al., 1991; Roberts et al., 1992; Wilson, 2009). We conclude therefore that the minor difference in surface gravity between Earth and Venus cannot explain the considerable contrast in volcano relief.

3.1.2. Viscosity of extruded lava flows

On Earth, high-viscosity lavas are better able to construct a tall volcanic edifice than low-viscosity lavas, which tend to travel much greater distances from the vent (e.g., Harris and Rowland, 2009). Although the bulk composition of Earth and Venus are similar (Bougher et al., 1997), the substantial influence of water content on the viscosity of melts (e.g., Dingwell et al., 1996) means that if Venusian melts are anhydrous (dry) then the lavas erupted onto its surface should have a higher viscosity than their Terran counterparts. It is possible that the Venusian mantle is about an order of magnitude more viscous than that of Earth, based on the assumption that Venusian melts are anhydrous and derived from an anhydrous mantle (Kaula, 1990; Nimmo and McKenzie, 1996; Mackwell et al., 1998). However, and as outlined above, recent data that suggest a hydrated Martian mantle (McCubbin et al., 2012) demand a reappraisal of the assumption that the Venusian mantle is anhydrous. Indeed, the vast majority of basaltic lava flows on the Venusian surface are of a similar spatial magnitude and thickness to the flows observed in basaltic large igneous provinces (LIPs) on Earth (e.g., Columbia River and Deccan Traps; Wilson, 2009); this similarity, together with the similar surface gravity of Earth and Venus, implies a similar basaltic flow viscosity. We also note that an increase in temperature results in a decrease in melt viscosity (Hess and Dingwell, 1996; Giordano et al., 2008), even for anhydrous melts (Hess et al., 2001). Therefore, if Venusian lavas are indeed anhydrous, the high temperature of the Venusian surface may decrease their nominal eruptive viscosity to a value closer to lavas extruded on Earth. We conclude, therefore, that the difference in viscosity of erupted lavas cannot explain the difference in morphology between the volcanoes on Earth and Venus.

3.1.3. Response of the lithosphere to geological loads

An additional parameter that controls the height of a volcanic structure is the mechanical rigidity of the basement upon which the volcano is situated (Watts, 2001). The flexural rigidity of the lithosphere depends on its rheology such that a strong and brittle lithosphere is better adapted to support high-relief structures than a weak and ductile lithosphere (Watts, 2001). Indeed, a thick and predominantly brittle crust has been used to explain the presence of the ultra-high-relief volcanoes on Mars (Turcotte et al., 1981; Heap et al., 2017a), with the mechanical response of the Martian crust even influencing the eruptive behaviour of these shield volcanoes (Byrne et al., 2013).

We contend that the experimental rock deformation data collated in Figs. 3 and 4 provide a simple explanation as to why Venus hosts volcanoes that, although perhaps as voluminous, are wider and of lower relief than those on Earth. On a global scale, high-relief structures cannot be supported on Venus to the same extent as they are on Earth due to the dominantly ductile Venusian crust. Recent analogue modelling by Byrne et al. (2013) is consistent with this conclusion. This prediction further suggests that the volcanic topographic highs on Venus (e.g., Maat Skadi Montes) may be relatively young, because our model predicts that high-relief structures on Venus will force the underlying lithosphere to yield over geological timescales (according to the models presented by Byrne et al. (2013); see also Smrekar and Solomon (1992) and Herrick et al. (2005)). Large volcanoes may even evolve into corona-like structures over time, evidenced by the number of volcano-corona 'hybrids' on the Venusian surface (e.g., Atai Mons; Grindrod et al., 2006). We also note that the downflexing of the lithosphere beneath a volcano imposes a constrictional strain upon the edifice, manifest as imbricate shortening structures arrayed around its flanks (Byrne et al., 2009, 2013). Unfortunately, the flanks of Venusian volcanoes are not sufficiently resolved with currently available data to test this hypothesis (full resolution Magellan topographic imagery has a resolution of about 100 m; Herrick et al., 2005).

3.2. Implications for volcanic character

The dominant mode of magma migration through Earth's crust (in terms of volume) is via fractures (e.g., Gudmundsson, 2006). The experimental data collated here suggest that, on Venus, faulting could be restricted to shallow depths (i.e., 2–12 km) (Fig. 4). Similar to Earth (Burov and Gerya, 2014), a rising mantle-derived melt on Venus will pond and spread laterally, underplating the crust at depths greater than that of the BDT (as shown in Fig. 5a–c for Venus). However, based on our depth estimates for the BDT on Venus (Fig. 4), the mechanism by which magmas on Venus can continue to migrate towards the BDT is through buoyancy-driven diapirism. Importantly, however, the lengthscale

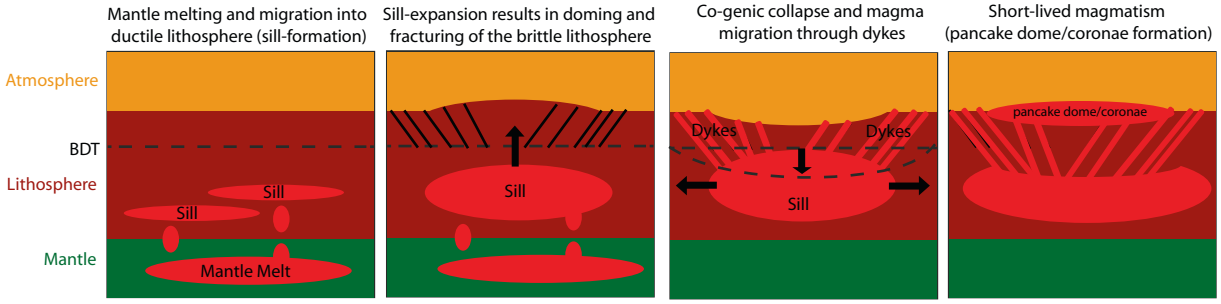

Fig. 5. The formation of coronae on Venus. This cartoon depicts sill emplacement and growth, followed by uplift and faulting of the crust above the brittle-ductile transition (BDT). The schematic also shows how this only leads to volcanism after the magma chamber makes physical contact with faults (see text for more details; not to scale). Arrows indicate directions of main differential stresses.

for magma migration by diapirism is considerably shorter than migration through dykes (Rubin, 1995; Gudmundsson, 2002, 2006, 2011; Petford, 2003) and diapirs will inevitably pond and create sills due to a stress-related equilibrium when the forces driving ascent are equal (or less than) the forces acting against ascent (i.e., crystallisation increasing viscosity) – unless more magma is added to further drive ascent via buoyancy-driven diapirism. Therefore, if magma transport through the lower to middle Venusian crust is dominated by diapirism, then a lower fraction of crust-situated melt can reach the surface and erupt, relative to Earth. Occasionally however, a sill may form that is large enough to generate enough uplift to initiate faulting in the brittle crust, creating a set of concentric vertical faults (see Galgana et al., 2013). If the magma reaches these faults (or vice versa) then melts can propagate upwards, forming ring-dikes or arachnoids (Head et al., 1992; Donahue and Russell, 1997; Basilevsky and Head, 2003; Wilson, 2009). Should it reach the surface, this melt will erupt as lava, and we conceptually show how this can result in the formation of the curious coronae features on Venus in Fig. 5.

A combination of lateral flow and dyke-facilitated volcanism will cause the sill (magma chamber) to contract vertically, and this can cut off the magma supply to the surface as the collapsing brittle crust closes the fracture network. This may result in subsidence beneath the forming or formed coronae with either negative or positive relief (both of which are commonly observed on Venus: Head et al., 1992; Donahue and Russell, 1997; Basilevsky and Head, 2003; Herrick et al., 2005; Wilson, 2009), which we argue is the result of variable ratios of the erupted lava to the amount of subsidence. If the magma supply from the plume to the crust is large enough and is active over sufficient timescales, then a shallow-flanked shield volcano could form (e.g., Maat Mons), the vertical growth of which is likely tempered by the inability of the predominantly ductile Venusian crust to support high-relief structures (due to its low flexural rigidity). However, if the magma chamber (sill) cannot connect with the faults, because the sill has stalled below the BDT, then surface eruption will not ensue. In this eventuality, grabens (*fossae* and *lineae*), fractures, scarps (*rupes*), or troughs will form, tectonic landforms common to the Venusian surface (Head et al., 1992; Donahue and Russell, 1997; Basilevsky and Head, 2003; Wilson, 2009).

Most volcanic systems on Earth show complex magmatic plumbing with several reservoirs situated at different depths. However, most primary mantle melts that reach the Earth's crust form sill-like magma chambers at the base of the crust (defined as primary magma chambers) and are typically found at depths considerably greater than 10 km (Kelley and Barton, 2008; Stroncik et al., 2009; Becerril et al., 2013). Therefore, on Earth, most shallow magma chambers are connected to a deeper primary magma chamber at depths of >10 km (Hill et al., 2009; Michon et al., 2015). This magma system architecture suggests that magma ponds at the crust–mantle boundary on Earth. Therefore, if Venusian melts form magma chambers at similar depth, or at a similar depth with respect to the stratigraphy of the crust (i.e., the crust–mantle boundary), as predicted for shallow magma chambers (Wilson and Head, 1994), then those chambers will be hosted below the BDT (predicted to occur between 2 and 12 km on Venus: see Fig. 4a–c), restricting magma mobility to the short lengthscales typical of diapirism (Rubin, 1995; Gudmundsson, 2002, 2006, 2011; Petford, 2003).

We can therefore predict, albeit qualitatively, that a greater proportion of magmatism on Venus does not result in volcanism, but instead results in plutonism, than on Earth. Indeed, lava flow unit thickness estimates from Magellan topographic data suggest that coronae are probably underlain by large magma bodies that are not emptied during eruption (Grindrod et al., 2010). Any crustal thickening in areas of high magmatic activity should thus be compensated by delamination back into the mantle with or without crustal uplift (Smrekar and Stofan, 1997; Ghail, 2015). To test the hypothesis that plutonism is favoured over volcanism on Venus (relative to Earth), we will now compare differences in volcanic flux on Earth and Venus with the available geochemical data.

4. Measuring the volcanic eruptive flux of Venus and Earth

Finding a suitable metric to compare the eruptive fluxes of Venus and Earth is challenging. For example, there is a large uncertainty for both the longevity and frequency of Venusian volcanism due to the lack of reliable chronostratigraphic or radiogenic isotopic data for the Venusian surface (Head et al., 1992; Basilevsky and Head, 2003; Kreslavsky et al., 2015). However, there is evidence that Venus has experienced some voluminous volcanism in the past, coined 'global resurfacing events'. The model for catastrophic volcanic resurfacing is based on the relatively few (*ca.* 1000) impact craters, and is thought to have occurred between 300 Ma and 1 Ga (e.g., McKinnon et al., 1997). Assuming a frequency of resurfacing episodes that declined with the rate of heat generation (based on K–Th–U systematics of the mantle), Kaula (1991) proposed that there could have been eight resurfacing events over Venus' 4.56 Ga history. Volcanism on Venus appears to be mostly quiescent between these resurfacing events, which are either random or occurring roughly once every 0.5 Ga (Kaula, 1991). If in fact magmatism during these largely passive periods does not result in extrusive volcanism, then by our inference it may instead be manifest as massive magmatic underplating of basaltic melts at the base of the crust and subsequent plutonism in the crust, possibly followed by delamination back into the mantle (Smrekar and Stofan, 1997).

An important and poorly constrained parameter is the thermal structure of the Venusian interior. Nimmo and McKenzie (1997, 1998) cite the composition (specifically the FeO abundance) of the basaltic rocks analysed by the Venera and Vega landers to argue that the potential temperature of the Venusian mantle was similar to the Earth's during the emplacement of these rocks. Note, the FeO data used by Nimmo and McKenzie (1997, 1998) are by no means absolute or accurate (they have large uncertainties), but these are the only data presently available and future missions are required to provide an improved insight. Nevertheless, they do provide a quantitative model with which to demonstrate the point. Since these basalts are between 300 and 800 Ma one must calculate the mantle temperature for the present day; this is because resurfacing events would have cooled the Venusian upper mantle, which would have been followed by an increase in temperature due to U–Th–K decay and thermal insulation by the crust. Nimmo and McKenzie (1997, 1998) concluded that it is unlikely that the Venusian mantle increased in temperature by more than 200 °C over 800 Ma. Hence, these workers proposed an upper limit of 1500 °C for the potential temperature of the present-day Venusian mantle (Nimmo and McKenzie, 1998). This temperature is below the solidus for water-undersaturated peridotite (Kohlstedt et al., 1996; Hirschmann, 2006), and so melt production would be restricted to adiabatic melting of thermochemical plumes rising through the mantle (e.g., such as the Hawaiian plume on Earth; Morgan, 1971).

A key feature of the conceptual model presented here is that, all else being equal, the volcanic eruptive flux of Venus should be lower than that of Earth. Since we cannot rely on estimates of volcanic flux from chronostratigraphic methods, we must look elsewhere. For example, the chemistry of a planet's atmosphere is a passive recorder of surface and subsurface processes – including volcanism (e.g., Mather, 2008; Gaillard and Scaillet, 2014; Mikhail and Sverjensky, 2014). Therefore, if Venus has experienced

a lower volcanic eruptive flux, relative to Earth, over its geological history then this will have left a geochemical fingerprint in the chemistry of the Venusian atmosphere. Therefore, we focus here on the stable isotopes of argon, principally ^{36}Ar, ^{38}Ar, and ^{40}Ar, as useful tools for investigating the origin of volatiles (with ^{38}Ar/^{36}Ar) and the degassing history (with ^{40}Ar/^{36}Ar) of Venus. This is because [1] there are data for the ^{40}Ar/^{36}Ar and ^{38}Ar/^{36}Ar ratios for the atmospheres of Earth, Mars, Venus, and solar wind (Porcelli and Pepin, 2003), and [2] ^{36}Ar and ^{38}Ar are primordial isotopes whereas ^{40}Ar is produced from the decay of ^{40}K, with a half-life of 1.25 Ga, meaning that ^{40}Ar in planetary atmospheres can be used to derive information regarding the degassing of planetary interiors (e.g., Halliday, 2013).

5. Validating the model: argon isotope data

Despite the dearth of missions into and below the Venusian atmosphere over the past 40 years, there are valuable data for the major and minor element geochemistry of the Venusian atmosphere, including argon isotope ratios. Indeed, argon isotopes have been previously used to inform on the evolution of Venus (e.g., Istomin et al., 1980; Hoffman et al., 1980a,b; Turcotte and Schubert, 1988; Kaula, 1990, 1991; Namiki and Solomon, 1998; Porcelli and Pepin, 2003; Mikhail and Sverjensky, 2014; Halliday, 2013; O'Rourke and Korenaga, 2015).

In December 1978, six gas analysers (four mass spectrometers and two gas chromatographers) provided *in-situ* measurements of the Venus atmospheric chemical and isotopic composition (summarised by Hoffman et al., 1980a). The Soviet Union's Venera 11 and 12 landers (Istomin et al., 1979) and the United States Pioneer Venus entry probe (Hoffman et al., 1980a) determined the argon isotope composition of the lower Venusian atmosphere (below the altitude limit of isotopic homogenisation). Importantly, these two independent measurements provided a ^{38}Ar/^{36}Ar ratio within error of one another (summarised by Hoffman et al., 1980b). The similarity for the ^{38}Ar/^{36}Ar ratios for Earth and Venus is indicative of a shared source of volatile elements (Fig. 6). We consider that the most surprising result of these measurements was that the ratio of radiogenic to primordial argon in the Venusian atmosphere was shown to be highly unradiogenic, with a ^{40}Ar/^{36}Ar ratio of only 1.03 ± 0.04. For comparison, most argon in the atmospheres of Earth and Mars is strongly radiogenic, with ^{40}Ar/^{36}Ar ratios of 298.56 and 1900 ± 300, respectively (Fig. 6). Below, we outline why atmospheric loss, Venus being a K-deficient planet, and diffusive degassing cannot explain the difference between the ^{40}Ar/^{36}Ar ratios of Earth and Venus. We then finish by proposing a solution (that leans on the notion of a shallow BDT for Venus), where we conclude that this discrepancy can be explained by a relatively low volcanic eruptive flux for Venus (compared to Earth).

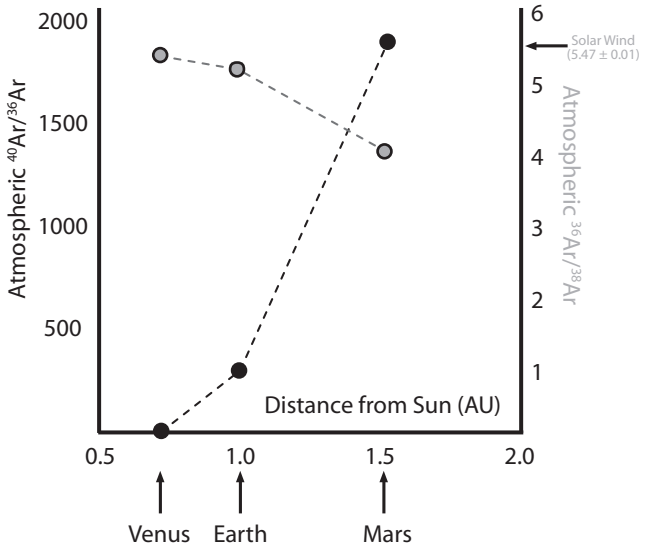

Fig. 6. The atmospheric argon isotope composition of Earth, Mars, and Venus (data from Istomin et al., 1979; Hoffman et al., 1980b; Porcelli and Pepin, 2003; Mahaffy et al., 2013). AU = Astronomical Units. Grey data points represent the relative abundance for the primordial argon isotopes (^{36}Ar/^{38}Ar), and black data points represent relative abundance for radiogenic argon over primordial argon (^{40}Ar/^{36}Ar).

5.1. The case against atmospheric loss to explain the unradiogenic argon

One of the principle mechanisms leading to stable isotope fractionation of atmosphere-forming elements is low-temperature atmospheric loss (i.e., hydrodynamic escape). This process induces mass dependant stable isotope fractionation, and therefore preferentially removes the lighter isotopes over the heavy isotopes (e.g., ^{36}Ar over ^{38}Ar, and ^{38}Ar over ^{40}Ar). This, in turn, means that the ^{38}Ar/^{36}Ar ratio would reflect substantial stable isotope fractionation if atmosphere loss to space were the sole reason for the unradiogenic ^{40}Ar/^{36}Ar ratio in the Venusian atmosphere (as is the case for Mars, i.e. Jakosky et al., 2017). Note, this is not the case for the Venusian and Terran datasets (Fig. 6). Hydrodynamic escape of ^{36}Ar cannot explain the low ^{40}Ar/^{36}Ar ratio of the Venusian atmosphere, because the ^{36}Ar/^{38}Ar data for the Venusian and Terran datasets are almost identical (i.e., 5.5 vs. 5.3; see Fig. 6), and Earth and Venus have very similar escape velocities for argon (*ca.* 12 and 13 km/s, respectively). Because Earth and Venus both show primordial ^{36}Ar/^{38}Ar ratios, both planets appear to share identical (isotopic) source materials (i.e., both are similar to their initial value recorded by solar wind: Porcelli and Pepin, 2003; Halliday, 2013). This in turn implies that both Earth and Venus had the same initial atmospheric ^{40}Ar/^{36}Ar ratio. A conundrum thus ensues: where is the missing ^{40}Ar in the Venusian atmosphere?

5.2. The case against Venus being a K-deficient planet

The unradiogenic ^{40}Ar/^{36}Ar ratio for the Venusian atmosphere also cannot be explained by proposing Venus to be a K-deficient planet, because the average observed K/U ratio in rocks on the Venusian surface is 7220 (akin to mid-ocean ridge basalts on Earth). Therefore, assuming an initial K/U and ^{38}Ar/^{36}Ar ratio for Earth and Venus, the present-day ^{40}Ar/^{36}Ar ratio of the Venusian atmosphere is not a reflection of the overall K abundance, but would therefore reflect either the flux of ^{40}Ar diffused or degassed out of the mantle and/or crust.

5.3. The case against efficient, diffusive degassing

The efficient transport of ^{40}Ar from the interior of a planet into its atmosphere can be, conceptually, achieved by diffusion. The entire Venusian crust is at a temperature above the closure temperature for argon in most silicate systems (Kelley and Wartho, 2000). However, efficient (or total) diffusion of ^{40}Ar through the crust cannot be proposed, because the Venusian atmosphere is strongly unradiogenic (for argon). This indicates that the Venusian crust has retained considerable ^{40}Ar produced continually over the age of the planet (4.56 Ga). The bulk silicate Venus (BSV) must therefore be saturated in ^{40}Ar. The lack of ^{40}Ar-diffusion at high Venusian surface temperatures can be explained by the lack of a chemical gradient. A buildup of ^{40}Ar in the crust above the closure

temperature does not necessarily mobilise the ^{40}Ar into the atmosphere. Buoyancy drives ascent, but pathways and mobilising agents are also required (note, gravity and physical inhibition are also acting as opposing forces). The lack of ^{40}Ar transport can be explained by a system that rapidly reaches equilibrium with the intergranular medium, despite diffusion coefficients great enough to model efficient mobilisation, conceptually (Cassata et al., 2011). Furthermore, mass-transfer along the grain boundary of silicates and oxides is limited to a very thin layer (*ca.* 1 nm; Joesten, 1991), so the bulk diffusivity should be reduced by the ratio of the thickness of the grain boundary to the diameter of the grain (Farvert and Yund, 1992). For a grain diameter of 0.1–1 mm, the diffusive lengthscales of argon is <1.2 km in 1 Ga. Since the lengthscale is less than the likely thickness of the Venusian crust (which is most certainly >1.2 km), the nominal diffusive flux of ^{40}Ar to the atmosphere is effectively zero over 1 Ga (Namiki and Solomon, 1998). Therefore, the nominal diffusive flux of ^{40}Ar to the atmosphere will be negligible over 4.5 Ga.

5.4. The case for a low volcanic eruptive flux on Venus relative to Earth

We propose volcanism as the main liberating agent for transporting ^{40}Ar to the Venusian atmosphere. During mantle melting on Earth and Venus, ^{40}K and ^{40}Ar are mobilised in melts, because they are both incompatible elements in primary mantle silicates, e.g., olivine (Chamorro et al., 2002; Brooker et al., 2003). This degassing implies that the strongly unradiogenic low ^{40}Ar/^{36}Ar ratio in the Venusian atmosphere is mirrored by a higher crustal excess of ^{40}Ar than is observed for the crust on Earth (which is known to contain excess ^{40}Ar: Allègre et al., 1996; Kelley, 2002). We argue that most of the ^{40}Ar transported in melts from the Venusian mantle is locked in plutons and stored within the Venusian crust, implying that there is a large excess of ^{40}Ar in the BSV. Our contention that a dominantly ductile Venusian crust (Fig. 4a–c) inhibits volcanism but results in abundant plutonism (relative to Earth; Fig. 7) forms a testable hypothesis: Venus should have degassed less ^{40}Ar, relative to Earth. Mars, for example, has a highly fractionated ^{36}Ar/^{38}Ar ratio of 4.1 (Porcelli and Pepin, 2003; Halliday, 2013), which reflects a substantial low-temperature loss of its atmosphere (Porcelli and Pepin, 2003; Halliday, 2013) (Fig. 6). Consequently, the present-day atmospheric ^{40}Ar/^{36}Ar ratios of Earth and Venus will reflect their relative efficiencies in ^{40}Ar degassing. The present-day Venusian atmosphere has a strongly unradiogenic ^{40}Ar/^{36}Ar ratio of 1.03 ± 0.04, compared with 298.56 for Earth (Kaula, 1991; Porcelli and Pepin, 2003; Halliday, 2013). However, the Venusian atmosphere also contains roughly two orders of magnitude more ^{36}Ar relative to Earth's atmosphere (Porcelli and Pepin, 2003). If we correct the ^{40}Ar/^{36}Ar ratio for Venus then the ^{40}Ar/^{36}Ar ratio of the Venusian atmosphere would be approximately 103, meaning Earth has degassed three times more ^{40}Ar than Venus. We view this implication here as a consequence of a higher rate of volcanism on Earth than on Venus. This is because the majority of Earth's volcanism is directly related to Earth's mobile-lid plate tectonic regime (Cottrell, 2015), but we argue that the high surface temperature and dearth of deep crustal faults on Venus also plays an important role. Therefore plutonism, rather than volcanism, is the dominant mode of magmatic activity on Venus (Fig. 7) and this is reflected in the unusually unradiogenic ^{40}Ar/^{36}Ar ratio observed in the Venusian atmosphere (Fig. 6).

6. Concluding remarks

We present here an experimentally-constrained and isotopically-supported conceptual model that predicts Venus to have been less volcanically active relative to Earth by a factor of three, in terms of eruptive flux. Since the volume of magma erupted cannot be directly quantified, we focus here on the degassing flux constrained by argon isotopes, which show that Earth has degassed three times more ^{40}Ar than Venus. We conclude that the reduced eruptive flux on Venus, compared to Earth, is the result of the hot Venusian climate, a factor that greatly impacts the dominant failure mode of, and therefore the method by which magma can travel up through, the Venusian crust. The higher rate of intraplate volcanic activity on Earth is exemplified by the observation that Earth's relatively young oceanic crust has seen the development of <100,000 individual volcanoes (i.e., seamounts) in <100 Ma, whereas Venus has only produced *ca.* 70,000 individual volcanoes over a much longer time period (700–1000 Ma) – a difference of an order of magnitude.

An interrogation of high pressure, high temperature experimental rock deformation data suggests that the unrelenting high temperature (460 °C) of the Venusian surface modifies the rheology of the Venusian crust such that the dominant failure mode within the Venusian crust is ductile. These data highlight that the BDT on Venus could be as shallow as 2–12 km (Fig. 4), while the same method yields a realistic estimate for the BDT on Earth of ~25–27 km (Fig. 3). The implications of a dominantly ductile Venusian crust are twofold. First, the flexural rigidity of the Venusian lithosphere will be low, inhibiting the formation of high-relief volcanoes (via lithospheric flexure). We further note that the low flexural rigidity of the Venusian lithosphere may not just impact volcano morphology, but also the global hypsometric profile of Venus (Fig. 1). We therefore speculate that the low standard devi-

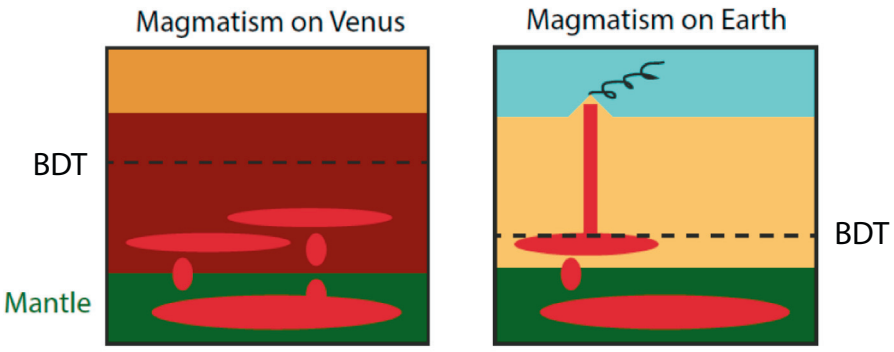

Fig. 7. Schematic illustration showing the relative differences for magma transport within the lithosphere on Earth and Venus. The cartoon shows that primary magma chambers on Venus rely on diapirism to move towards the surface, leading to stagnation and crystallisation (on average). Conversely for Earth, primary magma chambers can force dyking in the overlying (brittle) lithosphere and initiate volcanism.

ation of the Venusian surface is also the consequence of its hot climate. Second, magma delivery to the surface through fractures (i.e., dykes)—the dominant transport mechanism of magma to shallow crustal levels on the telluric planets (e.g., Wilson and Head, 1994; Gudmundsson, 2006)—will be impeded on Venus. Our conceptual model therefore predicts that most magma on Venus will stall in the crust as sills, rather than be erupted at the surface: plutonism, rather than volcanism, is the dominant mode of magmatic activity on Venus (Fig. 7). Importantly, these implications are supported by the atmospheric argon isotope ratios for Earth and Venus, which indicate that volcanic degassing, and therefore volcanic flux, has been three times lower on Venus than on Earth over the past 4.5 Ga (Fig. 6).

Our conceptual model falls short in describing, for example, the formation histories for the Venusian continents, Aphrodite Terra and Ishtar Terra (which, speculatively, could be the result of isostatic rebound before the global resurfacing event, or crustal delamination of the lower lithosphere back into the mantle, or a presently unknown mechanism; Smrekar and Stofan, 1997; Ghail, 2015). We also highlight that our conceptual model assumes various similarities between Earth and Venus, such as similar mantle convective regimes, which may not be strictly true (e.g., Johnson and Richards, 2003; Robin et al., 2007). Nevertheless, our model offers a viable explanation for the difference in volcano morphology between Earth and Venus (i.e., the presence of coronae) and the relative quiescence of volcanism on Venus compared to Earth (i.e., the order of magnitude difference in the rate of intraplate volcano formation between Earth and Venus). Furthermore, a Venusian BDT as shallow as predicted here also implies that faulting through the vertical lengthscale of the crust is hindered. Therefore, the hot climate of Venus may also inhibit the formation of the plate tectonic boundaries that sub-divide the crust (Foley et al., 2012; Bercovici and Ricard, 2014). Our study highlights another example of the complex interplay between climate and geodynamics.

Acknowledgements

We acknowledge stimulating discussions on argon geochemistry with Simon Kelley, Chris Ballentine, Colin Jackson, and Peter Barry, and with Richard Ghail on the tectonic history of Venus. We also acknowledge critical comments by Nicolas Le Corvec, Paul Byrne, two anonymous reviewers, and the editorial handling of Mark Jellinek that enabled us to improve this manuscript. M.J. Heap acknowledges funding from an Initiative d'Excellence (IDEX) "Attractivité" grant (VOLPERM), funded by the University of Strasbourg (France). The idea for this paper was conceived at Souk Kitchen (Bristol) the morning after the wedding of Jonathan Bruce Hanson and Jessica Shields. All of the data used in this manuscript are cited in the reference list.

References

Addington, E.A., 2001. A stratigraphic study of small volcano clusters on Venus. Icarus 149, 16–36.
Adelinet, M., Fortin, J., Schubnel, A., Guéguen, Y., 2013. Deformation modes in an Icelandic basalt: from brittle failure to localized deformation bands. J. Volcanol. Geoth. Res. 255, 12–25.
Airey, M.W., Mather, T.A., Pyle, D.M., Glaze, L.S., Ghail, R.C., Wilson, C.F., 2015. Explosive volcanic activity on Venus: the roles of volatile contribution, degassing, and external environment. Planet. Space Sci. 113, 33–48.
Al-Harthi, A.A., Al-Amri, R.M., Shehata, W.M., 1999. The porosity and engineering properties of vesicular basalt in Saudi Arabia. Eng. Geol. 54, 313–320.
Allègre, C.J., Hofmann, A., O'Nions, K., 1996. The Argon constraints on mantle structure. Geophys. Res. Lett. 23, 3555–3557.
Apuani, T., Corazzato, C., Cancelli, A., Tibaldi, A., 2005. Physical and mechanical properties of rock masses at Stromboli: a dataset for volcano instability evaluation. Bull. Eng. Geol. Environ. 64, 419–431.
Basilevsky, A.T., Head, J.W., 2003. The surface of Venus. Rep. Prog. Phys. 66, 1699–1734.
Baud, P., Klein, E., Wong, T.-F., 2004. Compaction localization in porous sandstones: spatial evolution of damage and acoustic emission activity. J. Struct. Geol. 26 (4), 603–624.
Bauer, S.J., Friedman, M., Handin, J., 1981. Effects of water-saturation on strength and ductility of three igneous rocks at effective pressures to 50 MPa and temperatures to partial melting. In: The 22nd U.S. Symposium on Rock Mechanics (USRMS), Cambridge, MA, June 29–July 2, 1981.
Bauer, S.J., Handin, J., 1983. Thermal expansion and cracking of three confined water-saturated igneous rocks to 800 °C. Rock Mech. Rock Eng. 16, 181–198.
Becerril, L., Galindo, I., Gudmundsson, A., Morales, J.M., 2013. Depth of origin of magma in eruptions. Sci. Rep. 2762. http://dx.doi.org/10.1038/srep02762.
Bell, D.R., Rossman, G.R., 1992. Water in the Earth's mantle: the role of nominally anhydrous minerals. Science 255, 1391–1397.
Benson, P.M., Thompson, A.B., Meredith, P.G., Vinciguerra, S., Young, R.P., 2007. Imaging slow failure in triaxially deformed Etna basalt using 3D acoustic-emission location and X-ray computed tomography. Geophys. Res. Lett. 34, L03303. http://dx.doi.org/10.1029/2006GL028721.
Bercovici, D., Ricard, Y., 2014. Plate tectonics, damage and inheritance. Nature 508, 513–516.
Bolfan-Casanova, N., Keppler, H., Rubie, D.C., 2000. Water partitioning between nominally anhydrous minerals in the MgO–SiO_2–H_2O system up to 24 GPa: implications for the distribution of water in the Earth's mantle. Earth Planet. Sci. Lett. 182, 209–221.
Bougher, S.W., Hunten, D.M., Phillips, R.J. (Eds.), 1997. Venus II. University of Arizona Press, Tucson.
Brace, W.F., Paulding, B.W., Scholz, C.H., 1966. Dilatancy in the fracture of crystalline rocks. J. Geophys. Res. 71, 3939–3953.
Brantut, N., Heap, M.J., Meredith, P.G., Baud, P., 2013. Time-dependent cracking and brittle creep in crustal rocks: a review. J. Struct. Geol. 52, 17–43.
Brooker, R.A., Du, Z., Blundy, J.D., Kelley, S.P., Allan, N.L., Wood, B.J., Chamorro, M., Wartho, J.-A., Purton, J.A., 2003. The 'zero charge' partitioning behaviour of noble gases during mantle melting. Nature 423, 738–741.
Brown, C.D., Grimm, R.E., 1997. Tessera deformation and the contemporaneous thermal state of the plateau highlands, Venus. Earth Planet. Sci. Lett. 147, 1–10.
Brown, C.D., Grimm, R.E., 1999. Recent tectonic and lithospheric thermal evolution of Venus. Icarus 139, 40–48.
Bullock, M.A., Grinspoon, D.H., 2001. The recent evolution of climate on Venus. Icarus 150, 19–37.
Burov, E., Gerya, T., 2014. Asymmetric three-dimensional topography over mantle plumes. Nature 513, 85–89.
Burt, J.D., Head, J.W., 1992. Thermal buoyancy on Venus: underthrusting vs. subduction. Geophys. Res. Lett. 19, 1707–1710.
Byrne, P., van Wyk de Vries, B., Murray, J., Troll, V., 2009. The geometry of volcano flank terraces on Mars. Earth Planet. Sci. Lett. 281, 1–13.
Byrne, P.K., Holohan, E.P., Kervyn, M., van Wyk de Vries, B., Troll, V.R., Murray, J.B., 2013. A sagging-spreading continuum of large volcano structure. Geology 41, 339–342.
Campbell, B.A.P.G., Rogers, 1994. Bell Regio, Venus—integration of remote-sensing data and terrestrial analogs for geologic analysis. J. Geophys. Res. Lett.: Planets 99, 21153–21171.
Caristan, Y., 1982. The transition from high temperature creep to fracture in Maryland diabase. J. Geophys. Res. 87, 6781–6790.
Carr, M.H., Head, J.W., 2010. Geologic history of Mars. Earth Planet. Sci. Lett. 294, 185–203.
Carr, M.H., Head, J.W., 2015. Martian surface/near-surface water inventory: sources, sinks, and changes with time. Geophys. Res. Lett. 42, 726–732.
Cassata, W.S., Renne, P.R., Shuster, D.L., 2011. Argon diffusion in pyroxenes: implications for thermochronometry and mantle degassing. Earth Planet. Sci. Lett. 304, 407–416.
Chamorro Perez, E.M., Brooker, R.A., Wartho, J.A., Wood, B.J., Kelley, S.P., Blundy, J.D., 2002. Ar and K partitioning between clinopyroxene and silicate melt to 8 GPa. Geochim. Cosmochim. Acta 66, 507–519.
Cottrell, E. 2015. Global Distribution of Active Volcanoes. In Volcanic Hazards, Risks, and Disasters, Ed. Papale, P. Elsevier, 1–14.
Crumpler, L.S., Head, J.W., Campbell, D.B., 1986. Orogenic belts on Venus. Geology 14, 1031–1034.
Dingwell, D.B., Romano, C., Hess, K.U., 1996. The effect of water on the viscosity of haplogranitic melt under P-T-X conditions relevant to silicic volcanism. Contrib. Miner. Petrol. 124, 19–28.
Donahue, T.M., 1999. New analysis of hydrogen and deuterium escape from Venus. Icarus 141, 226–235.
Donahue, T.M., Russell, C.T., 1997. The Venus atmosphere and ionosphere and their interaction with the solar wind: an overview. In: Bougher, S.W., Hunten, D.M., Phillips, R.J. (Eds.), Venus II. University of Arizona Press, Tucson, pp. 3–31.
Duclos, R., Paquet, J., 1991. High-temperature behaviour of basalts—role of temperature and strain rate on compressive strength and K_{IC} toughness of partially glassy basalts at atmospheric pressure. Int. J. Rock Mech. Mining Sci. Geomech. Abstr. 28, 71–76.
Ernst, R.E., 2007. Mafic–ultramafic large igneous provinces (LIPs): importance of the pre-Mesozoic record. Episodes 30, 108–114.
Esposito, L.W., 1984. Sulfur dioxide: episodic injection shows evidence for active Venus volcanism. Science 223, 1072–1074.
Fagents, S.A., Wilson, L., 1995. Explosive volcanism on Venus: transient volcanic explosions as a mechanism for localized pyroclast dispersal. J. Geophys. Res.: Planets 100, 26327–26338.

Farvert, J.R., Yund, R.A., 1992. Oxygen diffusion in a fine-grained quartz aggregate with wetted and non-wetted microstructures. J. Geophys. Res. 97, 14017–14029.

Fegley, B., Prinn, R.G., 1989. Estimation of the rate of volcanism on Venus from reaction rate measurements. Nature 337, 55–58.

Foley, B.J., Bercovici, D., Landuyt, W., 2012. The conditions for plate tectonics on super-Earths: inferences from convection models with damage. Earth Planet. Sci. Lett. 331, 281–290.

Gaillard, F., Scaillet, B., 2014. A theoretical framework for volcanic degassing chemistry in a comparative planetology perspective and implications for planetary atmospheres. Earth Planet. Sci. Lett. 403, 307–316.

Galgana, G.A., Grosfils, E.B., McGovern, P.J., 2013. Radial dike formation on Venus: insights from models of uplift, flexure and magmatism. Icarus 225, 538–547.

Ghail, R., 2015. Rheological and pertrological implications for a stagnant lid regime on Venus. Planet. Space Sci. 113, 2–9.

Ghail, R.C., Wilson, L. 2013. A pyroclastic flow deposit on Venus. Geological Society Special Publications, 401, London.

Ghent, R., Hansen, V.L., 1999. Structural and kinematic analysis of Eastern Ovda Regio, Venus: implications for crustal plateau formation. Icarus 139, 116–136.

Giordano, D., Russell, J.R., Dingwell, D.B., 2008. Viscosity of magmatic liquids: a model. Earth Planet. Sci. Lett. 271, 123–134.

Glaze, L.S., Baloga, S.M., Wimert, J., 2011. Explosive volcanic eruptions from linear vents on Earth, Venus, and Mars: comparisons with circular vent eruptions. J. Geophys. Res.: Planets 12, 116–128.

Griggs, D.T., Turner, F.J., Heard, H.C. 1960. Deformation of rocks at 500 to 800 °C. In: Griggs, D.T., Handin, J.W., (Eds.), Rock Deformation, Geol. Soc. Amer., Mem. 79, pp. 39–104.

Grimm, R.E., 1994. Recent deformation rates on Venus. J. Geophys. Res.: Planets 99, 23163–23171.

Grimm, R.E., Solomon, S.C., 1988. Viscous relaxation of impact crater relief on Venus: constraints on crustal thickness and thermal gradient. J. Geophys. Res.: Solid Earth 93, 11911–11929.

Grindrod, P.M., Hoogenboom, T., 2006. Venus: the corona conundrum. Astron. Geophys. 47, 3–16.

Grindrod, P.M., Stofan, E.R., Brian, A.W., Guest, J.E., 2006. The geological evolution of Atai Mons, Venus: a volcano-corona 'hybrid'. J. Geol. Soc. London 163, 265–275.

Grindrod, P.M., Stofan, E.R., Guest, J.E., 2010. Volcanism and resurfacing on Venus at the full resolution of Magellan SAR data. Geophys. Res. Lett. 37. http://dx.doi.org/10.1029/2010GL043424.

Grosfils, E.B., Head, J.W., 1994. The global distribution of giant radiating dike swarms on Venus: implications for the global stress state. Geophys. Res. Lett. 21, 701–704.

Grosfils, E.B., Long, S.M., Venechuk, E.M., Hurwitz, D.M., Richards, J.W., Kastl, B., Drury, D.E., Hardin, J., 2011. Geologic Map of the Ganiki Planitia Quadrangle (V-14), Venus [Map] Scientific Investigations Map 3121. U.S. Geological Survey.

Gudmundsson, A., 2002. Emplacement and arrest of dykes and sheets in central volcanoes. J. Volcanol. Geoth. Res. 116, 279–298.

Gudmundsson, A., 2006. How local stresses control magma-chamber ruptures, dyke injections, and eruptions in composite volcanoes. Earth Sci. Rev. 79, 1–31.

Gudmundsson, A., 2011. Rock fractures in geological processes. Cambridge University Press. ISBN: 978-0-521-86392-6.

Hacker, B.R., Christie, J.M., 1991. Experimental deformation of a glassy basalt. Tectonophysics 200, 79–96.

Halliday, A.N., 2013. The origins of volatiles in the terrestrial planets. Geochim. Cosmochim. Acta 105, 146–171.

Hansen, V.L., Willis, J.J., 1996. Structural analysis of a sampling of tesserae: implications for Venus geodynamics. Icarus 123, 296–312.

Hansen, V.L., Willis, J.J., 1998. Ribbon Terrain Formation, Southwestern Fortuna Tessera, Venus: implications for lithosphere evolution. Icarus 132, 321–343.

Harris, A.J.L., Rowland, S.K. 2009. Effusion rate controls on lava flow length and the role of heat loss: a review. In: Thordarson, T., Self, S., Larsen, G., Rowland, S.K., Hoskuldsson, A. (Eds.), Studies in Volcanology: The Legacy of George Walker. Special Publications of IAVCEI, Geological Society of London, 2, 33–51.

Head, J.W., Solomon, S.C., 1981. Tectonic evolution of the terrestrial planets. Science 213, 62–76.

Head, J.W., Wilson, L., 1992. Magma reservoirs and neutral buoyancy zones on Venus: implications for the formation and evolution of volcanic landforms. J. Geophys. Res. 97, 3877–3903.

Head, J.W., Crumpler, L.S., Aubele, J.C., Guest, J.E., Saunders, R.S., 1992. Venus volcanism: classification of volcanic features and structures, associations, and global distribution from Magellan data. J. Geophys. Res. 97, 13153–13197.

Heap, M.J., Vinciguerra, S., Meredith, P.G., 2009. The evolution of elastic moduli with increasing damage during cyclic stressing of a basalt from Mt, Etna volcano. Tectonophysics 471, 153–160.

Heap, M.J., Baud, P., Meredith, P.G., Vinciguerra, S., Bell, A.F., Main, I.G., 2011. Brittle creep in basalt and its application to time-dependent volcano deformation. Earth Planet. Sci. Lett. 307, 71–82.

Heap, M.J., Farquharson, J.I., Baud, P., Lavallée, Y., Reuschlé, T., 2015. Fracture and compaction of andesite in a volcanic edifice. Bull. Volcanol. 77, 55. http://dx.doi.org/10.1007/s00445-015-0938-7.

Heap, M.J., Byrne, P., Mikhail, S., 2017a. Low surface gravitational acceleration of Mars results in a thick and weak lithosphere: implications for topography, volcanism, and hydrology. Icarus 281, 103–114.

Heap, M.J., Violay, M., Wadsworth, F.B., Vasseur, J., 2017b. From rock to magma and back again: The evolution of temperature and deformation mechanism in conduit margin zones, Earth Planet. Sci. Lett. 463, 92–100.

Herrick, R.R., Dufek, J., McGovern, P.J., 2005. Evolution of large shield volcanoes on Venus. J. Geophys. Res. 110. http://dx.doi.org/10.1029/2004JE002283.

Hess, K.U., Dingwell, D.B., 1996. Viscosities of hydrous leucogranitic melts: a non-Arrhenian model. Am. Mineral. 81, 1297–1300.

Hess, P.C., Head, J.W., 1990. Derivation of primary magmas and melting of crustal materials on Venus: some preliminary petrogenetic considerations. Earth Moon Planet. 50–51, 57–80.

Hess, K.U., Dingwell, D.B., Gennaro, C., Mincione, V., 2001. Viscosity-temperature behavior of dry melts in the Qz-Ab-Or system. Chem. Geol. 174, 133–142.

Hill, G.J., Caldwell, T.G., Heise, W., Chertkoff, D.G., Bibby, H.M., Burgess, M.K., Cull, J. P., Cas, R.A.F., 2009. Distribution of melt beneath Mount St Helens and Mount Adams inferred from magnetotelluric data. Nat. Geosci. 211, 785–789.

Hirschmann, M.M., 2006. Water, melting, and the Earth deep H_2O cycle. Annu. Rev. Earth Planet. Sci. 34, 629–653.

Hoek, E., Bieniawski, Z.T., 1965. Brittle fracture propagation in rock under compression. Int. J. Fract. 1, 137–155.

Hoffman, J.H., Oyama, V.I., von Zahn, U., 1980a. Measurements of the Venus lower atmosphere composition: a comparison of results. J. Geophys. Res. 85, 7871–7881.

Hoffman, J.H.Hodges., Jr, R.R., Donahue, T.M., McElroy, M.B., 1980b. Composition of the Venus lower atmosphere from the Pioneer Venus mass spectrometer. J. Geophys. Res. 85, 7882–7890.

Hunten, D.M., 1993. Atmospheric evolution of the terrestrial planets. Science 259, 915–920.

Istomin, V.G., Grechnev, K.V., Kochnev, V.A. 1979. Pisma v Astronomicheskii Zhurnal, vol. 5, pp. 211–216 (Soviet Astronomy Letters, vol. 5, pp. 113–115, Trans.). (Original work published 1979).

Istomin, V.G., Grechnev, K.V., Kochnev, V.A., 1980. Mass Spectrometer Measurements of the Composition of the Lower Atmosphere of Venus. COSPAR Colloquia Series, Space Research — Proceedings of the Open Meetings of the Working Groups on Physical Sciences of the Twenty-Second Plenary Meeting of COSPAR Bangalore, India 29 May – 9 June 1979, 20, 215–218.

Ivanov, M.A., Head, J.W., 2013. The history of volcanism on Venus. Planet. Space Sci. 84, 66–92.

Jakosky, B.M., Slipski, M., Benna, M., Mahaffy, P., Elrod, M., Yelle, R., Stone, S., Alsaeed, N., 2017. Mars' atmospheric history derived from upper-atmosphere measurements of $^{38}Ar/^{36}Ar$. Science. 355, 1408–1410.

Jellinek, A.M., Lenardic, A., Manga, M., 2002. The influence of interior mantle temperature on the structure of plumes: heads for Venus, tails for the Earth. Geophys. Res. Lett. 29. http://dx.doi.org/10.1029/2001GL014624.

Joesten, R., 1991. Grain-boundary diffusion kinetics in silicate and oxide minerals, in Diffusion, Atomic Ordering, and Mass Transport, Advanced Physical Geochemistry, edited by J. Ganguly, vol. 8, pp. 345–395, Springer-Verlag, New York.

Johnson, C.L., Richards, M.A., 2003. A conceptual model for the relationship between coronae and large-scale mantle dynamics on Venus. J. Geophys. Res.: Planets 108 (E6). http://dx.doi.org/10.1029/2002JE001962.

Kaula, W.M., 1990. Venus: a contrast in evolution to Earth. Science 247, 1191–1196.

Kaula, W.M., 1991. Constraints on Venus evolution from radiogenic argon. Icarus 139, 32–39.

Kelley, S., 2002. Excess argon in K-Ar and Ar-Ar geochronology. Chem. Geol. 188, 1–22.

Kelley, D.F., Barton, M., 2008. Pressures of crystallization of Icelandic magmas. J. Petrol. 49, 465–492.

Kelley, S.P., Wartho, J.-A., 2000. Rapid kimberlite ascent and the significance of Ar-Ar ages in xenolith phlogopites. Science 289, 609–611.

Kohlstedt, D.L., Evans, B., Mackwell, S.J., 1995. Strength of the lithosphere: constraints imposed by laboratory experiments. J. Geophys. Res. 100, 17587–17602.

Kohlstedt, D.L., Keppler, H., Rubie, D.C., 1996. Solubility of water in the α, β and γ phases of (Mg, Fe)2SiO4. Contrib. Mineral. Petrol. 123, 345–357.

Krassilnikov, A.S., Head, J.W., 2003. Novae on Venus: geology, classification, and evolution. Journal of Geophyscial Research 108. http://dx.doi.org/10.1029/2002JE001983.

Krassilnikov, A.S., Kostama, V.-P., Aittola, M., Guseva, E.N., Cherkashina, O.S., 2012. Relation- ship of coronae, regional plains and rift zones on Venus. Planet. Space Sci. 68, 56–75.

Kreslavsky, M.A., Ivanov, M.A., Head, J.W., 2015. The resurfacing history of Venus: constraints from buffered crater densities. Icarus 250, 438–450.

Lécuyer, C., Simon, L., Guyot, F., 2010. Comparison of carbon, nitrogen and water budgets on Venus and the Earth. Earth Planet. Sci. Lett. 181, 33–40.

Leitner, J.J., Firneis, M.G. 2006. A review of Venusian surface heat flow estimates, AGU Chapman Conference on Exploring Venus as a Terrestrial Planet.

Mackwell, S.J., Zimmerman, M.E., Kohlstedt, D.L., 1998. High-temperature deformation of dry diabase with application to tectonics on Venus. J. Geophys. Res. 103, 975–984.

Mahaffy, P.R., Webster, C.R., Atreya, S.K., Franz, H., Wong, M., Conrad, P.G., Harpold, D., Jones, J.J., Leshin, L.A., Manning, H., Owen, T., Pepin, R.O., Squyres, S., Trainer, M., MSL Science Team, 2013. Abundance and Isotopic Composition of Gases in the Martian Atmosphere from the Curiosity Rover. Science 341, 263–266.

Marcq, E., Belyaev, D., Montmessin, F., Fedorova, A., Bertaux, J.-L., Vandaele, A.C., Neefs, E., 2011. An investigation of the SO_2 content of the venusian mesosphere using SPICAV-UV in nadir mode. Icarus 211, 58–69.

Mather, T.A., 2008. Volcanism and the atmosphere: the potential role of the atmosphere in unlocking the reactivity of volcanic emissions. Philos. Trans. Royal Soc. A 366, 4581–4595.

McCubbin, F.M., Hauri, E.H., Elardo, S.M., Vander Kaaden, K.E., Wang, J., Shearer Jr, C. K., 2012. Hydrous melting of the martian mantle produced both depleted and enriched shergottites. Geology 40, 683–686.
McGill, G.E., 2000. Geologic Map of the Sappho Patera Quadrangle (V-20), Venus [Map] Geologic Investigations Series I-2637. U.S. Geological Survey.
McGovern, P.J., Galgana, G.A., Verner, K.R., Herrick, R.R., 2014. New constraints on volcano-tectonic evolution of large volcanic edifices on Venus from stereo topography-derived strain estimates. Geology 42, 59–62.
McKenzie, D., Ford, P.G., Liu, F., Pettengill, G.H., 1992. Pancakelike domes on Venus. J. Geophys. Res. 97, 15967–15976.
McKinnon, W.B., Zahnle, K.J., Ivanov, B.A., Melosh, H.J., 1997. Cratering on Venus: models and Observations. In: Bougher, S.W., Hunten, D.M., Phillips, R.J. (Eds.), Venus II. University of Arizona Press, Tucson, pp. 969–1015.
Menéndez, B., Zhu, W., T-f, Wong., 1996. Micromechanics of brittle faulting and cataclastic flow in Berea sandstone. J. Struct. Geol. 18, 1–16.
Michon, L., Ferrazzini, V., Di Muro, A., Villeneuve, N., Famin, V., 2015. Rift zones and magma plumbing system of Piton de la Fournaise volcano: how do they differ from Hawaii and Etna? J. Volcanol. Geoth. Res. 303, 112–129.
Mikhail, S., Sverjensky, D.A., 2014. Nitrogen speciation in upper mantle fluids and the origin of Earth's nitrogen-rich atmosphere. Nat. Geosci. 7, 816–819.
Morgan, W.J., 1971. Convection plumes in the lower mantle. Nature 230, 42–43.
Mouginis-Mark, P.J., 2016. Geomorphology and volcanology of Maat Mons, Venus. Icarus 277, 433–441.
Namiki, N., Solomon, S.C., 1998. Volcanic degassing of argon and helium and the history of crustal production on Venus. J. Geophys. Res. 103, 3655–3677.
Nimmo, F., McKenzie, D., 1996. Modelling plume-related uplift, gravity and melting on Venus. Earth Planet. Sci. Lett. 145, 109–123.
Nimmo, F., McKenzie, D., 1997. Convective thermal evolution of the upper mantles of Earth and Venus. Geophys. Res. Lett. 24, 1539–1542.
Nimmo, F., McKenzie, D., 1998. Volcanism and tectonics on Venus. Ann. Rev. Earth Planet. Sci. 26, 23–51.
O'Rourke, J., Korenaga, J., 2015. Thermal evolution of Venus with argon degassing. Icarus 260, 128–140.
Ougier-Simonin, A., Fortin, J., Guéguen, Y., Schubnel, A., Bouyer, F., 2011. Cracks in glass under triaxial conditions. Int. J. Eng. Sci. 49, 105–121.
Petford, N., 2003. Rheology of grantic magmas during ascent and emplacement. Annu. Rev. Earth Planet. Sci. 31, 399–427.
Pettengill, G.H., Ford, P.G., Johnson, W.T.K., Raney, R.K., Soderblom, L.A., 1991. Magellan: radar performance and data products. Science 252, 260–265.
Phillips, R.J., Hanson, V.L., 1998. Geological evolution of Venus: rises, plains, plumes, and plateau. Science 279, 1492–1497.
Plescia, J.B., 2004. Morphometric properties of Martian volcanoes. J. Geophys. Res. 109 (E3). http://dx.doi.org/10.1029/2002JE002031.
Pollack, J.B., Toon, O.B., Whitten, R.C., Boese, R., Ragent, B., Tomasko, M., Esposito, L., Travis, L., Wiedman, D., 1980. Distribution and source of the UV absorption in Venus' atmosphere. J. Geophys. Res. 85, 8141–8150.
Porcelli, D., Pepin, R.O., 2003. The Origin of noble gases and major volatiles in the terrestrial planets. Treat. Geochem., 319–347
Roberts, K.M., Guest, J.E., Head, J.W., Lancaster, M.G., 1992. Mylitta Fluctus, Venus: rift-related, centralized volcanism and the emplacement of large-volume flow units. J. Geophys. Res.: Planets 97, 15991–16015.
Robin, C.M.I., Jellinek, M., Thayalan, V., Lenardic, A., 2007. Transient mantle convection on Venus: the paradoxical coexistence of highlands and coronae in the BAT region. Earth Planet. Sci. Lett. 256, 100–111.
Rocchi, V., Sammonds, P.R., Kilburn, C.R.J., 2004. Fracturing of Etnean and Vesuvian rocks at high temperatures and low pressures. J. Volcanol. Geoth. Res. 132, 137–157.
Rubin, A.M., 1995. Propagation of magma-filled cracks. Annu. Rev. Earth Planet. Sci. 23, 287–336.
Ruiz, J., 2007. The heat flow during the formation of ribbon terrains on Venus. Planet. Space Sci. 55, 2063–2070.
Rutter, E., 1986. On the nomenclature of mode of failure transitions in rocks. Tectonophysics 122, 381–387.
Schaefer, L.N., Kendrick, J.E., Oommen, T., Lavallée, Y., Chigna, G., 2015. Geomechanical rock properties of a basaltic volcano. Front. Earth Sci. http://dx.doi.org/10.3389/feart.2015.00029.
Scholz, C.H., 1968. Microfracturing and the inelastic deformation of rock in compression. J. Geophys. Res. 73, 1417–1432.
Schubert, G., Bercovici, D., Glatzmaier, G.A., 2010. Mantle dynamics in Mars and Venus: influence of an immobile lithosphere on three-dimensional mantle convection. J. Geophys. Res. 95, 14105–14129.
Schultz, R.A., 1993. Brittle strength of basaltic rock masses with applications to Venus. J. Geophys. Res.: Planets 98, 10883–10895.
Sclater, J.G., Jaupart, C., Galson, D., 1980. The heat flow through oceanic and continental crust and the heat loss of the Earth. Rev. Geophys. Space Phys. 18, 269–311.
Shalygin, E.V., Markiewicz, W.J., Basilevsky, A.T., Titov, D.V., Ignatiev, I.V., Head, J.W., 2015. Active volcanism on Venus in the Ganiki Chasma rift zone. Geophys. Res. Lett. 42, 4762–4769.
Shimada, M., 1986. Mechanism of deformation in a dry porous basalt at high pressures. Tectonophysics 121, 153–173.
Shimada, M., Yukutake, H., 1982. Fracture and deformation of silicate rocks at high pressures in a cubic press. Adv. Earth Planetary Sci. 12, 193–205.
Shimada, M., Ito, K., Cho, A., 1989. Ductile behavior of a fine-grained porous basalt at room temperature and pressures to 3 GPa. Phys. Earth Planetary Interiors 55, 361–373.
Smith, D.K., 1996. Comparison of the shapes and sizes of seafloor volcanoes on Earth and "pancake" domes on Venus. J. Volcanol. Geoth. Res. 73, 47–64.
Smith, R., Sammonds, P., Tuffen, H., Meredith, P.G., 2011. Evolution of the mechanics of the 2004–2008 Mt. St. Helens lava dome with time and temperature. Earth Planet. Sci. Lett. 307, 191–200.
Smrekar, S.E., Solomon, S.C., 1992. Gravitational spreading of high terrain in Ishtar Terra, Venus. J. Geophys. Res.: Planets 97, 16121–16148.
Smrekar, S.E., Stofan, E.R., 1997. Corona formation and heat loss on Venus by coupled upwelling and delamination. Science 277, 1289–1294.
Smrekar, S.E., Stofan, E.R., Mueller, N., Treiman, A., Elkins-Tanton, L., Helbert, J., Piccioni, G., Drossart, P., 2010. Recent hotspot volcanism on Venus from VIRTIS emissivity data. Science 328, 605–608.
Smyth, J.R., Frost, D.J., Nestola, F., Holl, C.M., Bromiley, G., 2006. Olivine hydration in the deep upper mantle: effects of temperature and silica activity. Geophys. Res. Lett. 33, L15301.
Solomatov, V.S., Moresi, S.-N., 1996. Stagnant lid convection on Venus. J. Geophys. Res.: Planets 101, 2156–2202.
Solomon, S.C., Head, J.W., 1982. Mechanisms for lithospheric heat transport on Venus: implications for tectonic style and volcanism. J. Geophys. Res.: Solid Earth 87, 9236–9246.
Solomon, S.C., Head, J.W., 1984. Venus banded terrain: tectonic models for band formation and their relationship to lithospheric thermal structure. J. Geophys. Res.: Solid Earth 89, 6885–6897.
Squyres, S.W., Janes, D.M., Baer, G., Bindschadler, D.L., Schubert, G., Sharpton, V.L., Stofan, E.R., 1992. The morphology and evolution of coronae on Venus. J. Geophys. Res.: Planets 97, 13611–13634.
Stofan, E.R., Sharpton, V.L., Schubert, G., Baer, G., Bindschadler, D.L., Janes, D.M., Squyres, S.W., 1992. Global distribution and characteristics of coronae and related features on Venus: implications for origin and relation to mantle processes. J. Geophys. Res.: Planets 97, 13347–13378.
Stofan, E.R., Smerkar, S.E., Bindschadler, D.L., Senske, D.A., 1995. Large topographic rises on Venus: implications for mantle upwelling. J. Geophys. Res.: Planets 100, 23317–23327.
Stroncik, A., Klügel, A., Hansteen, T.H., 2009. The magmatic plumbing system beneath El Hierro (Canary Islands): constraints from phenocrysts and naturally quenched basaltic glasses in submarine rocks. Contrib. Miner. Petrol. 157, 593–607.
Taylor, S.R., McLennan, S (eds.). 2009. Planetary Crusts: their Composition, Origin and Evolution. Cambridge University Press, 400p.
Thornhill, G.D., 1993. Theoretical modeling of eruption plumes on Venus. J. Geophys. Res.: Planets 98, 9107–9111.
Treiman, A.H., 2007. Geochemistry of Venus' surface: current limitations as future opportunities. Chapter in Exploring Venus as a Terrestrial Planet. AGU Monograph Series 176, 7–22.
Turcotte, D.L., 1993. An episodic hypothesis for Venusian tectonics. Journal of Geophyscial Research: Planets 98, 2156–2202.
Turcotte, D.L., 1995. How does Venus lose heat? J. Geophys. Res.: Planets 100, 16931–16940.
Turcotte, D.L., Schubert, G., 1988. Tectonic implications of radiogenic noble gases in planetary atmospheres. Icarus 74, 36–46.
Turcotte, D.L., Willemann, R.J., Haxby, W.F., Norberry, J., 1981. Role of membrane stresses in the support of planetary topography. J. Geophys. Res. 86, 3951–3959.
Turcotte, D.L., Morein, G., Roberts, D., Malamud, B.D., 1999. Catastrophic resurfacing and episodic subduction on venus. Icarus 139, 49–54.
Violay, M., Gibert, B., Mainprice, D., Evans, B., Dautria, J.-M., Azias, P., Pezard, P., 2012. An experimental study of the brittle-ductile transition of basalt at oceanic crust pressure and temperature conditions. J. Geophys. Res. http://dx.doi.org/10.1029/2011JB008884.
Violay, M., Gibert, B., Mainprice, D., Burg, J.-P., 2015. Brittle versus ductile deformation as the main control of the deep fluid circulation in oceanic crust. Geophys. Res. Lett. http://dx.doi.org/10.1002/2015GL063437.
Watts, 2001. Isostasy and Flexure of the Lithosphere. Cambridge University Press. ISBN 0 521 62272 7.
Wessel, P., 2001. Global distribution of seamounts inferred from gridded Geosat/ERS-1 altimetry. J. Geophys. Res. 106, 19431–19441.
Williams, C.A., Connors, C., Dahlen, F.A., Price, E.J., Suppe, J., 1994. Effect of the brittle-ductile transition on the topography of compressive mountain belts on Earth and Venus. J. Geophys. Res.: Solid Earth 99, 19947–19974.
Wilson, L., 2009. Volcanism in the solar system. Nat. Geosci. 2, 389–397.
Wilson, L., Head, J.W., 1983. A comparison of volcanic eruption processes on Earth, Moon, Mars, Io, and Venus. Nature 302, 663–669.
Wilson, L., Head, J.W., 1994. Mars: review and analysis of volcanic eruption theory and relationships to observed landforms. Rev. Geophys. 32, 221–263.
Wong, T.-f., David, C., Zhu, W., 1997. The transition from brittle faulting to cataclastic flow in porous sandstones: mechanical deformation. J. Geophys. Res. 102, 3009–3025.
Zhu, W., Baud, P., Vinciguerra, S., Wong, T-f. 2016. Micromechanics of brittle faulting and cataclastic flow in Mt. Etna basalt: micromechanics of deformation in basalt. J. Geophys. Res., DOI: 10.1002/2016JB012826.